

Regulation of senescence-associated secretory phenotypes in osteoarthritis by cytosolic UDP-GlcNAc retention and O-GlcNAcylation

Received: 27 April 2024

Accepted: 27 November 2024

Published online: 04 February 2025

 Check for updates

Donghyun Kang ^{1,2,12}, Jeeyeon Lee ^{1,2,12}, Geunho Yook^{1,2}, Sehan Jeong^{1,2}, Jungkwon Shin ^{1,2}, Mi-Sung Kim ¹, Yi-Jun Kim³, Hyeryeon Jung ⁴, Jinsung Ahn⁴, Tae Woo Kim⁵, Moon Jong Chang⁵, Chong Bum Chang⁶, Seung-Baik Kang⁵, Won Ho Yang ^{7,8}, Yong-ho Lee ^{8,9}, Jin Won Cho^{7,8}, Eugene C. Yi^{4,8}, Chanhee Kang ¹ & Jin-Hong Kim ^{1,2,8,10,11} ✉

UDP-GlcNAc serves as a building block for glycosaminoglycan (GAG) chains in cartilage proteoglycans and simultaneously acts as a substrate for O-GlcNAcylation. Here, we show that transporters for UDP-GlcNAc to the endoplasmic reticulum (ER) and Golgi are significantly downregulated in osteoarthritic cartilage, leading to increased cytosolic UDP-GlcNAc and O-GlcNAcylation in chondrocytes. Mechanistically, upregulated O-GlcNAcylation governs the senescence-associated secretory phenotype (SASP) by stabilizing GATA4 via O-GlcNAcylation at S406, which compromises its degradation by p62-mediated selective autophagy. Elevated O-GlcNAcylation in the superficial layer of osteoarthritic cartilage coincides with increased GATA4 levels. The topical deletion of *Gata4* in this cartilage layer ameliorates post-traumatic osteoarthritis (OA) in mice while inhibiting O-GlcNAc transferase mitigates OA by decreasing GATA4 levels. Excessive glucosamine-induced O-GlcNAcylation stabilizes GATA4 in chondrocytes and exacerbates post-traumatic OA in mice. Our findings elucidate the role of UDP-GlcNAc compartmentalization in regulating secretory pathways associated with chronic joint inflammation, providing a senostatic strategy for the treatment of OA.

Osteoarthritis (OA) is a leading cause of disability, imposing a large socioeconomic burden. OA affects 7% of the global population, and the number of patients living with the disease increased globally by 48% between 1990 and 2019 (Ref. 1). Multiple etiological risk factors, including aging, obesity, and mechanical overloads, contribute to the development and progression of OA. The progression of OA is characterized by cartilage degeneration and other pathological changes such as

subchondral bone sclerosis, osteophyte formation, and synovial inflammation.

Joints exposed to the risk factors of OA gradually accumulate senescent cells, which are mainly found in a superficial layer of the articular cartilage². Senescent chondrocytes reinforce senescence-associated secretory phenotypes (SASPs), comprising inflammatory mediators and matrix-degrading enzymes, thereby contributing to low-grade chronic inflammation in the joints²⁻⁴. Accordingly,

A full list of affiliations appears at the end of the paper. ✉ e-mail: jinhkim@snu.ac.kr

chondrocyte SASPs directly mediate osteoarthritic cartilage degeneration and further propagate secondary senescence to their surroundings such as the synovium, aggravating OA. Therefore, senostatics, an approach to modulate the production of SASPs, are a rational paradigm for treating OA.

Osteoarthritic cartilage degeneration primarily involves the loss of proteoglycan (PGs) from the cartilage matrix. Cartilage PGs, composed of elongated glycosaminoglycan (GAG) chains bound to core proteins, confer a unique load-bearing function to the articular joints⁵. Because uridine diphosphate N-acetylglucosamine (UDP-GlcNAc) is used as a building block of repeating disaccharide units for GAG chains, chondrocytes adequately maintain intracellular UDP-GlcNAc^{6,7}. UDP-GlcNAc also serves as a substrate for O-linked-N-acetylglucosaminylation (O-GlcNAcylation). O-GlcNAc transferase (OGT) catalyzes the addition of GlcNAc from UDP-GlcNAc to the serine or threonine residues of target proteins, while O-GlcNAcase (OGA) removes this post-translational modification^{8,9}. O-GlcNAcylation has been recognized as a crucial post-translational modification that integrates nutritional and metabolic sensing with the regulation of diverse cellular responses^{10,11}. Dysregulated O-GlcNAcylation has been associated with various human diseases, including cancer^{12–14} and chronic diseases such as type 2 diabetes mellitus (T2DM)¹⁵ and cardiovascular disease (CVD)¹⁶.

We undertook this study upon observing marked changes in the expression of transporters that may affect the intracellular distribution of UDP-GlcNAc during the development of senescence phenotypes. Our objective was to explore how shifts in UDP-GlcNAc compartmentalization could influence O-GlcNAcylation and key features of cellular senescence.

Here, we demonstrate UDP-GlcNAc compartmentalization as a distinct mode of controlling O-GlcNAcylation, directing chondrocyte secretory pathways from PG synthesis towards senescence-associated chronic inflammation. Our findings shed light on the stress-response mechanisms underlying the emergence of SASPs in chondrocytes, offering valuable insights for the development of senostatics as a rational approach for treating OA.

Results

Senescent chondrocytes exhibit altered intracellular UDP-GlcNAc flux

UDP-GlcNAc and UDP-N-acetylgalactosamine (UDP-GalNAc), capable of interconversion, are transported from the cytosol to the endoplasmic reticulum (ER) and the Golgi apparatus by a range of solute carrier family 35 (SLC35) transporters, including SLC35A2, SLC35A3, SLC35A5, SLC35B4, SLC35D1, and SLC35D2 (Supplementary Table 1). In the secretory organelles, the imported sugars are utilized in the synthesis of GAG-rich PGs. Because OA is primarily characterized by the loss of PG contents in cartilage, we sought to examine the expression of these transporters in OA or OA-associated transcriptome data available through the Gene Expression Omnibus (GEO) database. The expression of UDP-GlcNAc and UDP-GalNAc transporters were downregulated across multiple human OA transcriptome datasets (Fig. 1a). Similarly, their expression levels were consistently decreased in interleukin (IL)-1 β -treated chondrocytes (Fig. 1b) and various animal models of OA (Fig. 1c) compared with those of corresponding controls.

Senescent chondrocytes are implicated in the development of OA^{2,3}. DNA-damaging chemical agents such as doxorubicin or bleomycin, and ionizing radiation (IR) robustly caused the cellular senescence of human C28/I2 chondrocytes and primary cultured mouse chondrocytes, as marked by increased senescence-associated β -galactosidase (SA- β -Gal) positivity, reduced S-phase entry, upregulated expression of *CDKN1A* and *CDKN2A INK4A*, and downregulated expression of *LMNB1* (Fig. 1d, e and Supplementary Fig. 1). Principal component analysis (PCA) of chondrocyte transcriptomes revealed distinct profiles following bleomycin and doxorubicin treatments,

separating them from responses observed in vehicle- or IL-1 β -treated conditions (Supplementary Fig. 2a). Differentially expressed genes (DEGs) in bleomycin-treated and doxorubicin-treated chondrocytes showed considerable overlap (Supplementary Fig. 2b), commonly involving pathways related to DNA damage response, cell cycle arrest, and inflammation (Supplementary Fig. 2c, d).

Notably, the senescence-inducing stimuli commonly reduced the expression levels of *SLC35A3*, *SLC35B4*, *SLC35D1*, and *SLC35D2* in these cells (Fig. 1f, g and Supplementary Fig. 3a). We then measured the content of UDP-GlcNAc in the ER, Golgi apparatus, and cytosol of the chondrocytes, respectively. The total UDP-GlcNAc levels remained unaffected in human C28/I2 chondrocytes following the treatment with doxorubicin under a senescence-eliciting scheme (Fig. 1h). However, the senescence-inducing stimuli reduced UDP-GlcNAc levels in the ER and the Golgi apparatus while conversely elevating its content in the cytosol (Fig. 1h). The cytosolic accumulation of UDP-GlcNAc was similarly observed in senescent mouse chondrocytes with no significant alteration in total UDP-GlcNAc levels (Fig. 1i). In contrast, inhibition of the hexosamine biosynthetic pathway by targeting glutamine-fructose-6-phosphate transaminase (GFPT) using 6-diazo-5-oxo-L-norleucine (DON) reduced UDP-GlcNAc levels in the ER, Golgi, and cytosol simultaneously (Fig. 1h, i). These results collectively suggest that senescence-inducing stimuli alter the intracellular UDP-GlcNAc distribution by preferentially retaining it within the cytosol. This change in the UDP-GlcNAc redistribution further correlated with a decrease in the GAG content within the secreted PGs from senescent chondrocytes (Fig. 1j, k and Supplementary Fig. 3b). Meanwhile, no statistically significant changes in the expression of *OGT* and *OGA* were observed in OA cartilage (Supplementary Fig. 4a–c) or senescent chondrocytes (Supplementary Fig. 4d–f).

O-GlcNAcylation is associated with chondrocyte senescence in OA cartilage

Because cytosolic UDP-GlcNAc is used as a substrate for O-GlcNAcylation, we next explored whether the altered intracellular UDP-GlcNAc flux is correlated with the extent of O-GlcNAcylation in the OA-affected cartilage. The degree of O-GlcNAcylation was markedly elevated in OA-affected human cartilage but was marginal in undamaged regions of arthritic cartilage (Fig. 2a, b and Supplementary Fig. 5a, b). Notably, the expression of p16^{INK4a}, a biomarker of cellular senescence¹⁷, was highly colocalized in chondrocytes displaying O-GlcNAcylation signals such that their double positivity is significantly higher in OA-affected cartilage than in the undamaged counterparts (Fig. 2b and Supplementary Fig. 5b).

Given the cytosolic accumulation of UDP-GlcNAc in senescent chondrocytes (Fig. 1h, i), we further explored how senescence-inducing stimuli affect O-GlcNAcylation in primary cultured human and mouse chondrocytes. Following treatment with doxorubicin, human articular chondrocytes exhibited a markedly increased level of O-GlcNAcylation (Fig. 2c and Supplementary Fig. 5c). Similarly, primary mouse chondrocytes displayed a global increase in O-GlcNAcylation along with the onset of senescence following bleomycin treatment or long-term exposure to hydrogen peroxide (H₂O₂) (Fig. 2d, e).

We then questioned whether O-GlcNAcylation is necessary for the entry of chondrocytes into senescence. However, the bleomycin-induced increases in DNA damage and SA- β -Gal positivity were not alleviated by treatment with the OGT inhibitor ST045849 (Fig. 2f, g). Similarly, the expression of biomarkers associated with the permanent cell cycle arrest of senescent cells, *Cdkn1a* and *Cdkn2a Ink4a*, was not affected by O-GlcNAcylation (Fig. 2h). These results suggested that O-GlcNAcylation does not affect the entry of chondrocytes into senescence. Therefore, we next explored whether O-GlcNAcylation affects the development of SASPs as another major aspect of senescent cells^{3,18}.

Damage-induced senescence in human articular chondrocytes resulted in the expression of SASP factors, which was accompanied by the upregulation of GATA4, a transcription regulator governing

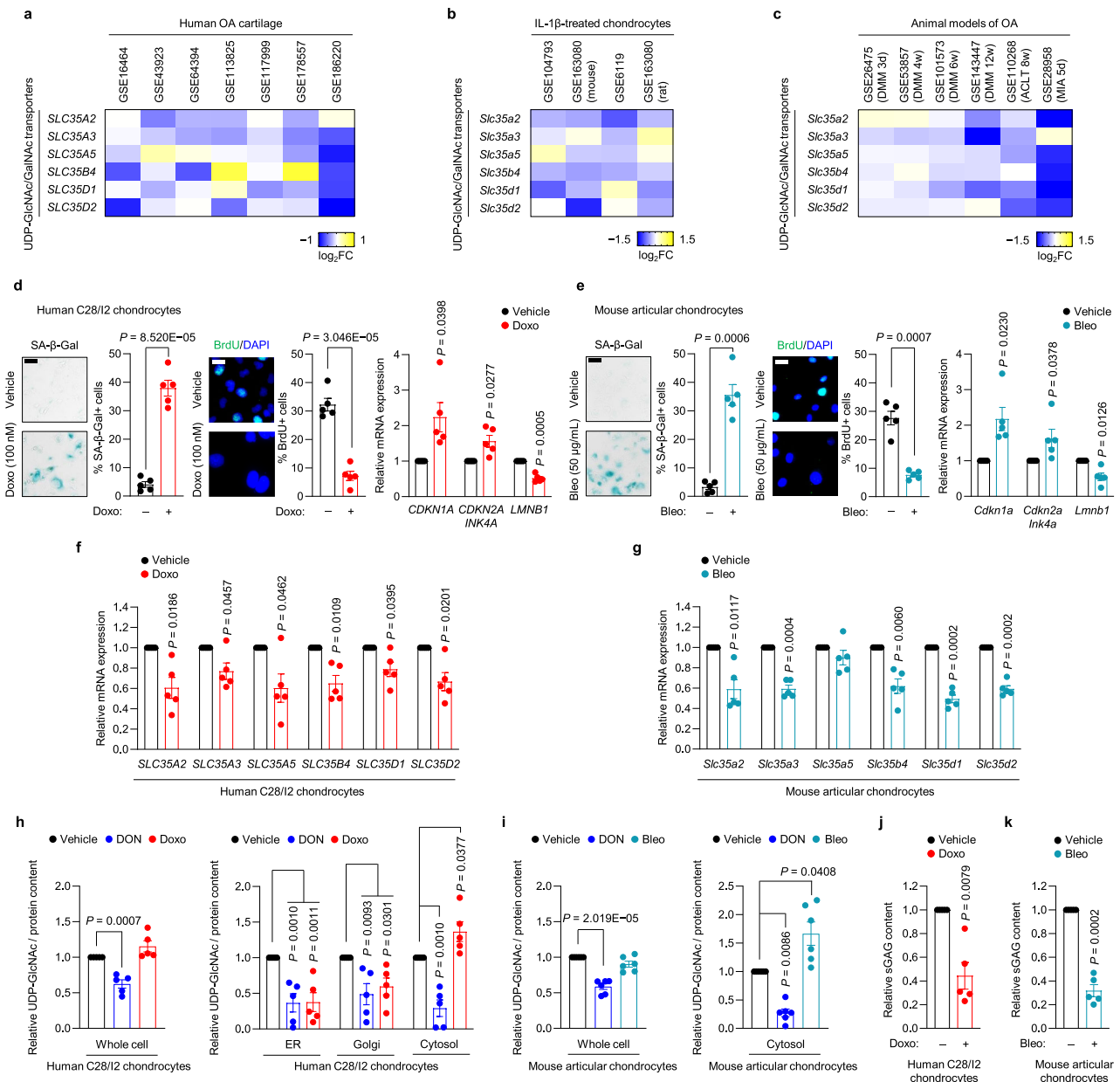
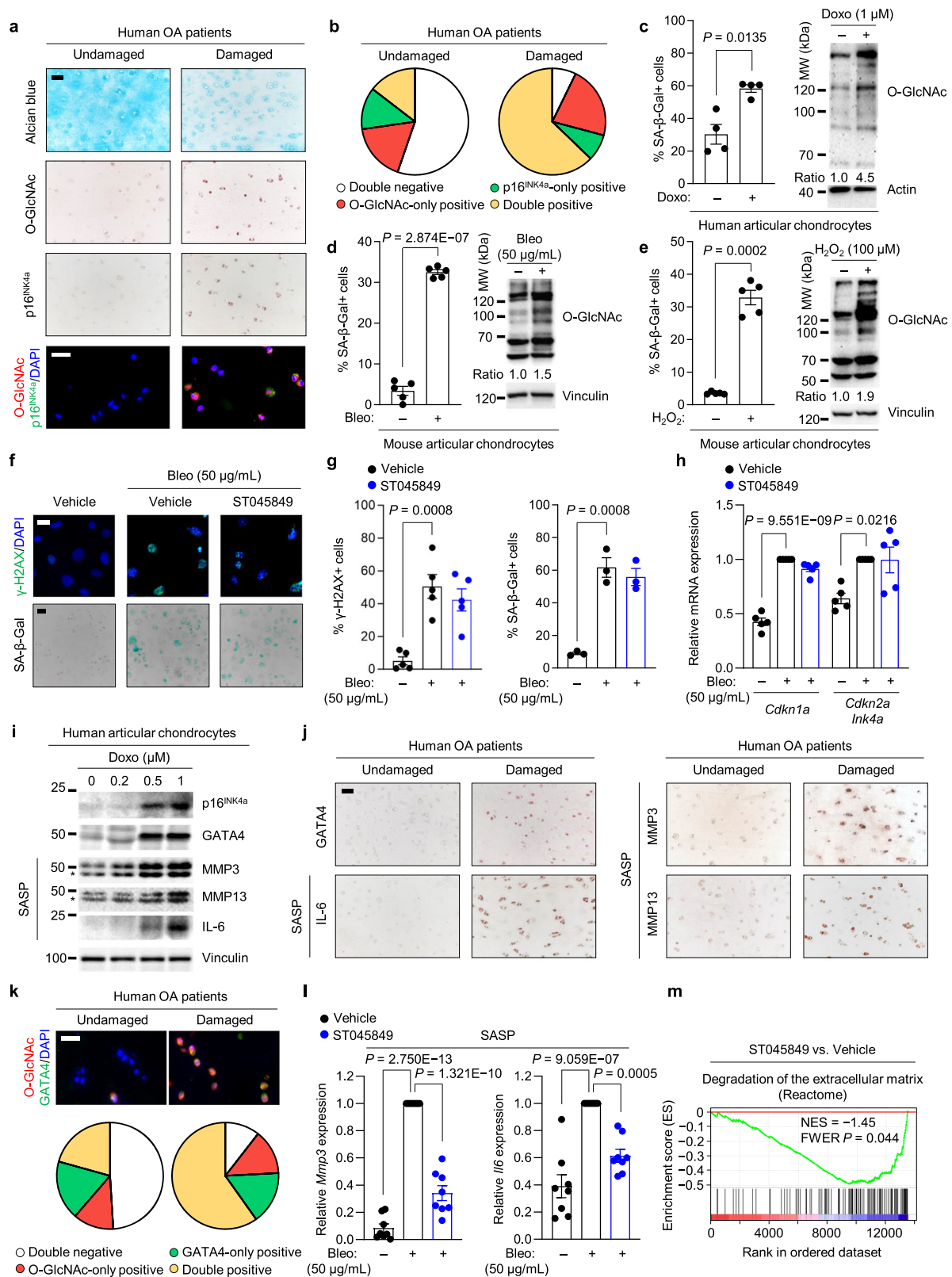


Fig. 1 | The expression of UDP-GlcNAc transporters is downregulated in OA-associated chondrocytes, correlating with cytosolic UDP-GlcNAc retention. **a–c** Fold change (FC) heatmap of the expression levels of transporters for UDP-GlcNAc and UDP-GalNAc in human OA cartilage and OA-relevant conditions. Public transcriptome datasets analyzed were generated from **(a)** human OA cartilage (GSE16464, GSE43923, GSE64394, GSE113825, GSE117999, GSE178557, and GSE186220), **(b)** IL-1 β -treated chondrocytes (GSE6119, GSE104793, and GSE163080), and **(c)** cartilage from OA models of mice (GSE26475, GSE53857, GSE101573, GSE110268, and GSE143447) and rats (GSE28958). **d**, **e** SA- β -Gal staining and quantification of SA- β -Gal positivity (left), representative images of immunofluorescence and quantification of BrdU incorporation (middle), and relative mRNA expression levels of CDK inhibitors or *Lmnbl1* (right) in **(d)** C28/I2 chondrocytes treated with 100 nM of doxorubicin ($n = 5$) or in **(e)** mouse chondrocytes treated

with 50 μ g/mL of bleomycin ($n = 5$). **f**, **g** Relative mRNA expression levels of transporters for UDP-GlcNAc and UDP-GalNAc in **(f)** C28/I2 chondrocytes treated with doxorubicin ($n = 5$) or in **(g)** mouse chondrocytes treated with bleomycin ($n = 5$). **h** Quantification of UDP-GlcNAc levels in the whole cell (left) and the ER, Golgi apparatus, and cytosol (right) of C28/I2 chondrocytes treated with vehicle, DON, or doxorubicin ($n = 5$). **i** Quantification of UDP-GlcNAc levels in the whole cell (left) and cytosol (right) of mouse chondrocytes treated with vehicle, DON, or bleomycin ($n = 6$). **j** Sulfated GAG (sGAG) release of C28/I2 chondrocytes treated with vehicle or doxorubicin measured using an sGAG assay ($n = 5$). **k** sGAG release of mouse chondrocytes treated with bleomycin ($n = 5$). Scale bars: **d**(left), **e**(left), 50 μ m, **d**(middle), **e**(middle), 25 μ m. **d–k** Data represent means \pm s.e.m. P values are from two-tailed t test (**d–g**, **j**, **k**) or one-way ANOVA followed by Dunnett's post-hoc test (**h**, **i**). Source data are provided as a Source Data file.

SASPs¹⁹ (Fig. 2i). Likewise, the expression levels of GATA4 and SASP factors were markedly elevated in OA-affected human cartilage as compared with those in the undamaged counterparts (Fig. 2j). GATA4 expression was highly co-localized with O-GlcNAcylation signals, leading to a significant increase in their double positivity in OA-affected articular cartilage compared to undamaged tissue (Fig. 2k and Supplementary Fig. 5a, d). Notably, inhibition of O-GlcNAcylation

effectively suppressed the expression of SASP factors in senescent chondrocytes (Fig. 2l and Supplementary Fig. 5e). Conversely, augmenting the extent of O-GlcNAcylation by treatment with the OGA inhibitor thiamet-G further enhanced SASP expression in senescent chondrocytes (Supplementary Fig. 5f). Because SASP is mainly comprised of matrix-degrading proteases and pro-inflammatory cytokines, we further examined how gene sets related to these annotations are



regulated in senescent chondrocytes at the whole-transcriptome level by suppressing O-GlcNAcylation. Gene set enrichment analysis (GSEA) revealed gene sets such as “degradation of the extracellular matrix”²⁰ and “positive regulation of cytokine production involved in inflammatory response”²¹ were negatively enriched in the transcriptome of senescent chondrocytes treated with the OGT inhibitor as compared with those treated with a vehicle control (Fig. 2m and Supplementary Fig. 5g). Collectively, our results indicate that stress-induced O-

GlcNAcylation is required for the full display of the SASP in senescent chondrocytes.

O-GlcNAcylation of GATA4 regulates its stability and transcriptional activity

Given the observed correlation between the degree of O-GlcNAcylation and expression of the SASP regulator GATA4 in the OA cartilage, we explored a possible mechanistic link between O-GlcNAcylation and the

Fig. 2 | Stress-induced O-GlcNAcylation regulates the senescence-associated secretory phenotype of chondrocytes in osteoarthritic cartilage. **a** Sections of human OA cartilage stained with Alcian blue and immunostained for O-GlcNAc and p16^{INK4a}. Representative co-immunofluorescence images of O-GlcNAc and p16^{INK4a}. **b** Pie charts showing the O-GlcNAc or p16^{INK4a} positivity from immunofluorescence in undamaged and damaged regions of human OA cartilage ($n = 6$). **c–e** Quantification of SA- β -Gal positivity and western blot for global O-GlcNAcylation in primary chondrocytes from **(c)** humans or **(d,e)** mice, treated with vehicle or **(c)** doxorubicin ($n = 4$), **(d)** bleomycin ($n = 5$), or **(e)** H₂O₂ ($n = 5$). **f, g** Immunofluorescence of γ -H2AX and SA- β -Gal staining in chondrocytes treated with bleomycin (50 μ g/mL) for 24 h, followed by treatment with vehicle (DMSO) or ST045849 (20 μ M) for 72 h. **(f)** Representative images and **(g)** quantification of γ -H2AX and SA- β -Gal positivity ($n = 5$, 3 respectively). **h** Relative mRNA levels of senescence markers in chondrocytes treated with bleomycin, followed by treatment with vehicle or ST045849 ($n = 5$).

i Western blot of p16^{INK4a}, GATA4, and SASPs in primary human chondrocytes treated with doxorubicin for 14 days. The asterisks indicate active form of the MMPs ($n = 4$). **j** Immunohistochemistry of GATA4 and SASP factors in human OA cartilage ($n = 3$). **k** Representative images (top) and pie charts (bottom) of O-GlcNAc or GATA4 positivity in human OA cartilage ($n = 6$). **l** Relative mRNA levels of SASP factors in chondrocytes treated with bleomycin for 24 h followed by treatment with vehicle or ST045849 for five days ($n = 8$). **m** GSEA of RNA-seq data using “Degradation of the extracellular matrix” gene set in chondrocytes treated with bleomycin, followed by treatment with vehicle or ST045849. Scale bars: **a(top),f(bottom)** **j**, 50 μ m, **a(bottom),f(top),k**, 25 μ m. **c–e,g,h,l** Data represent means \pm s.e.m. P values are from two-tailed t test (**c–e**), two-way ANOVA followed by Tukey’s post-hoc test (**g,h,l**), or one-tailed permutation test corrected for multiple comparisons with FWER (**m**). Source data are provided as a Source Data file.

regulation of GATA4. The cell-based co-immunoprecipitation assay indicated that GATA4 interacts with OGT (Fig. 3a). To examine whether GATA4 is O-GlcNAcylated, whole-cell lysates were precipitated with succinylated wheat germ agglutinin (sWGA) beads, which have high affinity for GlcNAc residues, and then probed against anti-GATA4. GATA4 was detected in sWGA precipitates, and the extent of the modifications substantially increased following treatment with thiamet-G (Fig. 3b). To directly detect the O-GlcNAc moiety in GATA4, exogenously expressed GATA4 was pulled down and subjected to immunoblotting with anti-O-GlcNAc. The O-GlcNAc modifications in GATA4 were highly detected in the presence of thiamet-G (Fig. 3c).

Next, we questioned whether O-GlcNAcylation is mechanistically coupled to the modulation of GATA4 activity. GATA4 is subjected to selective autophagy-mediated degradation in the absence of senescence-associated stimuli and, therefore, generally present at a basal level¹⁹. The global increase in O-GlcNAcylation substantially promoted the protein levels of GATA4 (Fig. 3d), which in turn led to an augmented GATA4-mediated transcriptional activity (Fig. 3e). Conversely, inhibition of O-GlcNAcylation resulted in downregulation of GATA4-mediated transcriptional activity (Fig. 3e). The cycloheximide (CHX) chase assay further demonstrated that the stability of GATA4 protein is markedly enhanced by increasing the extent of O-GlcNAcylation under thiamet-G treatment (Fig. 3f). In line with our observations that OGT inhibition suppresses GATA4 transcriptional activity (Fig. 3e), the expression of GATA4 target genes was negatively enriched in the transcriptome obtained from senescent chondrocytes treated with the OGT inhibitor ST045849 (Fig. 3g). Furthermore, treatment with ST045849 inhibited the bleomycin-induced expression of SASP factors in chondrocytes but had no additive inhibitory effect after *Gata4* silencing (Fig. 3h, i and Supplementary Fig. 6a). These results demonstrated that O-GlcNAcylation regulates SASP expression via the GATA4 pathway.

To map the O-GlcNAcylation sites in GATA4, we purified exogenously expressed GATA4, which was subjected to mass spectrometry (MS)-based proteomic analysis. This site-mapping experiment identified two O-GlcNAcylation sites: S212 located near an N-terminal zinc finger domain (217–241) and S406 adjacent to the intrinsically disordered region (409–428) (Supplementary Fig. 6b). To dissect the functional effects of these two evolutionarily conserved O-GlcNAcylation sites (Supplementary Fig. 6c), we generated a panel of mutant constructs of GATA4 in which the serine residues at 212 and 406 were replaced with alanines. We then explored how the loss of O-GlcNAcylation in GATA4 affects the protein stabilization induced by thiamet-G treatment. GATA4-S406A, but not GATA4-S212A, failed to respond to thiamet-G treatment, implicating a role of GATA4 O-GlcNAcylation at S406 in protecting against autophagy-mediated degradation (Fig. 3j). Because GATA4 is degraded by selective autophagy via its association with the p62 adaptor, we examined whether O-GlcNAcylation in GATA4 affects its association with p62. Indeed, thiamet-G treatment substantially diminished the binding between GATA4 and p62, accounting for its stabilization under this condition

(Fig. 3k and Supplementary Fig. 6d). In contrast, the association of GATA4-S406A with p62 was unaffected upon thiamet-G treatment (Fig. 3k), in line with our observation that the protein stability of this GATA4 mutant was unaffected by increasing the overall level of O-GlcNAcylation. Collectively, our results indicate that stress-induced O-GlcNAcylation stabilizes GATA4 by preventing its association with p62 and thus its inclusion in the lysosomal degradation pathway.

Genetic deletion of GATA4 in the superficial zone of the cartilage ameliorates OA in mice

To gain better insight into the relevance of this mechanism in a physiological context, we examined the expression patterns of O-GlcNAcylation and GATA4 in the knee joint cartilage of a post-traumatic OA mouse model. Immunohistochemical signals of O-GlcNAcylation and GATA4 were restricted to the superficial layer of the articular cartilage, with highly overlapping patterns between them (Fig. 4a). Because the role of GATA4 in chondrocytes during OA pathogenesis has not been determined, we generated tamoxifen (TMX)-inducible, chondrocyte-specific *Gata4* knockout mice, which were subjected to post-traumatic OA by surgical destabilization of the medial meniscus (DMM). The temporally-induced *Gata4* knockout in chondrocytes significantly ameliorated the development of OA manifestations, including cartilage destruction, subchondral bone sclerosis, osteophyte maturation, and synovitis (Fig. 4b, c and Supplementary Fig. 7a). We assessed OA-associated pain by measuring weight imbalance and mechanical allodynia between the surgically (sham or DMM) treated and untreated legs. These pain-driven behaviors were alleviated by the genetic deletion of *Gata4* in chondrocytes (Fig. 4d and Supplementary Fig. 7b).

Based on these results, we hypothesized that if the protective effect of *Gata4* knockout is manifested through the senostatic effect in senescent chondrocytes, topical deletion of *Gata4* within the superficial zone of the cartilage would be sufficient to exert protective effects on OA development. To test this hypothesis, we constructed a *Gata4*^{fl/fl}; *Prg4-CreER*^{T2} mouse line that allows for the temporally-induced knockout of *Gata4* in the superficial layer of the articular cartilage. The genetic deletion of *Gata4* in superficial chondrocytes diminished osteoarthritic cartilage destruction, subchondral bone sclerosis, osteophyte maturation, and synovial inflammation to a similar extent as observed in mice with cartilage-wide *Gata4* knockout (Fig. 4e, f). Microcomputed tomography (μ CT) scanning of the subchondral trabecular bone revealed a marked protective effect against OA-associated bone remodeling in *Gata4* knockout mice compared to that detected in the control mice following DMM surgery (Fig. 4g). At the molecular level, knockout of *Gata4* in the superficial zone of the knee cartilage in DMM-operated mice resulted in the suppression of matrix metalloproteinase 3 (MMP3), MMP13, and IL-6 expression, supporting the senostatic effects of targeting *Gata4* (Fig. 4h). Moreover, the expressions of senescence biomarkers (p16^{INK4a} and HMGB1) and the inflammation-independent SASP factor (HGF) were similarly

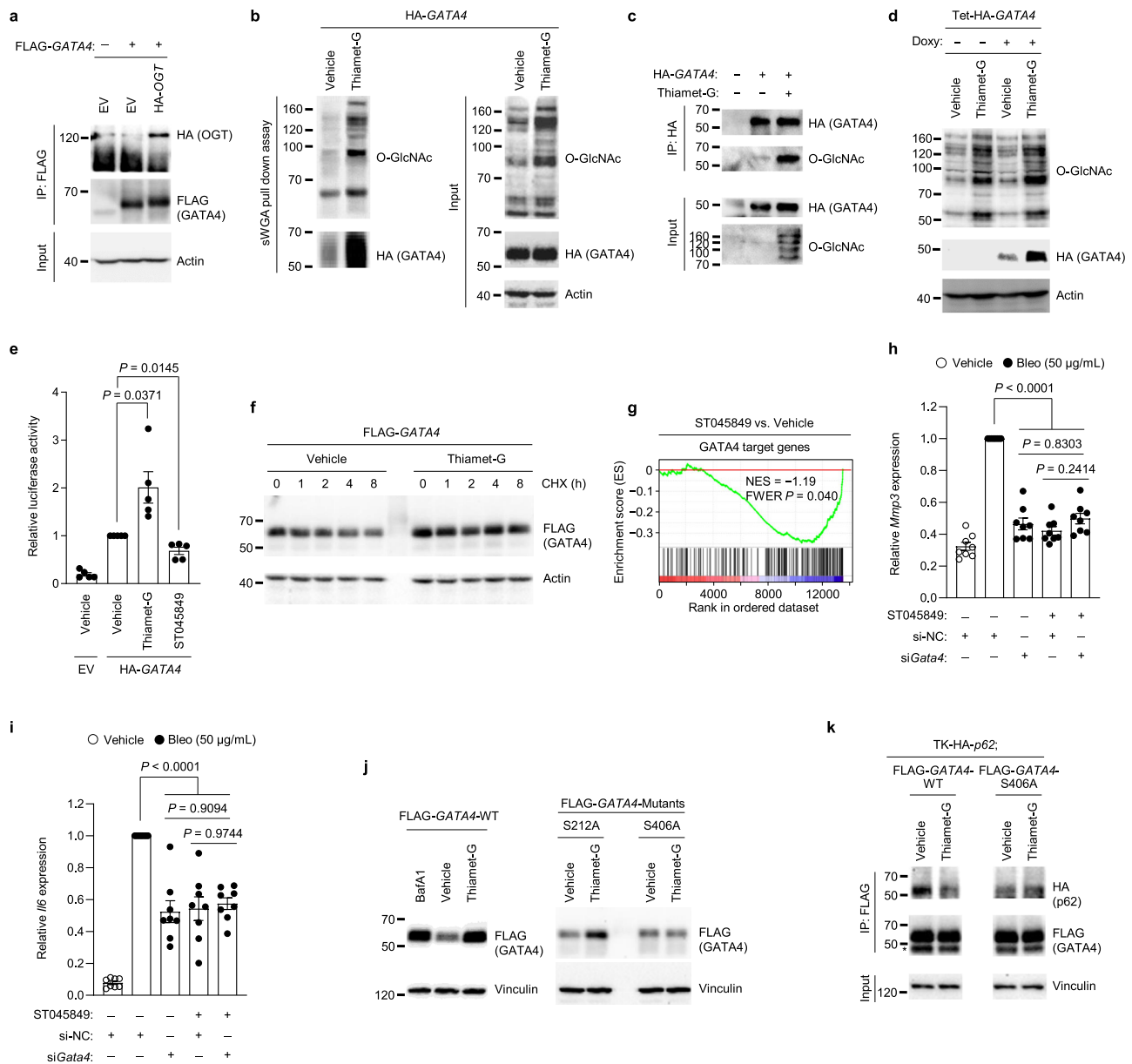


Fig. 3 | The O-GlcNAcylation of GATA4 prevents its degradation via selective autophagy, driving the expression of SASPs. a Co-immunoprecipitation of FLAG-tagged GATA4 with HA-tagged OGT in HEK293T ($n = 3$). **b** Immunoblot of pull-down using sWGA-conjugated agarose beads with or without thiamet-G treatment in HEK293T ($n = 3$). **c** Immunoblot of O-GlcNAcylation of HA-tagged GATA4 in HEK293T treated with vehicle or thiamet-G ($n = 3$). HA-tagged proteins were pulled down using anti-HA antibodies. MG132 (10 μ M) was applied for 6 h before lysis. **d** Immunoblot of GATA4 in HEK293T transfected with Tet-HA-GATA4 and treated with Doxy (1 μ g/mL) or left untreated, with or without thiamet-G (10 μ M) for 60 h ($n = 3$). **e** GATA reporter gene assay in HEK293T transfected with TK promoter-driven empty vector (EV) or HA-GATA4, followed by treatment with vehicle, thiamet-G, or ST045849 for 36 h ($n = 5$). **f** CHX chase analysis in HEK293T-FLAG-GATA4 treated with vehicle or thiamet-G (20 μ M) ($n = 3$). **g** GSEA of RNA-seq data from chondrocytes treated with bleomycin for 24 h, followed by vehicle or ST045849 for

five days, using “GATA4 target genes” gene set. **h, i** Relative mRNA levels of (**h**) *Mmp3* and (**i**) *Il6* in chondrocytes treated with bleomycin for 24 h followed by transfection with control or *Gata4* siRNAs, and treatment with vehicle or ST045849 for five days ($n = 8$). **j** Western blot in HEK293T transfected with FLAG-tagged GATA4 WT or mutants (S212A or S406A) with or without thiamet-G (20 μ M) for 48 h ($n = 3$). The Bafilomycin A1 (BafA1) treatment condition blocks autophagy-mediated protein degradation. **k** Co-immunoprecipitation of FLAG-tagged GATA4 WT or S406A mutant with HA-tagged p62 in HEK293T ($n = 3$). Cells were treated with vehicle or thiamet-G (20 μ M, 48 h) and BafA1 (50 nM, 24 h). The asterisk indicates IgG heavy chains. **e, h, i, j** Data represent means \pm s.e.m. *P* values are from two-tailed *t* test (**e**), one-tailed permutation test corrected for multiple comparisons with FWER (**g**), or two-way ANOVA followed by Tukey’s post-hoc test (**h, i**). Source data are provided as a Source Data file.

reduced, indicating an overall mitigation of OA-associated cellular senescence (Supplementary Fig. 7c). These senostatic effects were mirrored in senescent chondrocytes treated with *Gata4* siRNA (Supplementary Fig. 7d) or those exposed to the small-molecule GATA4 inhibitor NSC140905 (Refs. 22,23) (Supplementary Fig. 7e). Superficial chondrocyte-specific *Gata4* knockout mitigated the weight imbalance and mechanical allodynia induced by OA development

(Fig. 4i, j), suggesting effective management of OA-associated pain development.

Pharmacological targeting of the O-GlcNAc–GATA4 axis in post-traumatic OA in mice

Our findings indicated that O-GlcNAcylation promotes the stability of GATA4 (Fig. 3), which fosters SASPs in chondrocytes to enhance

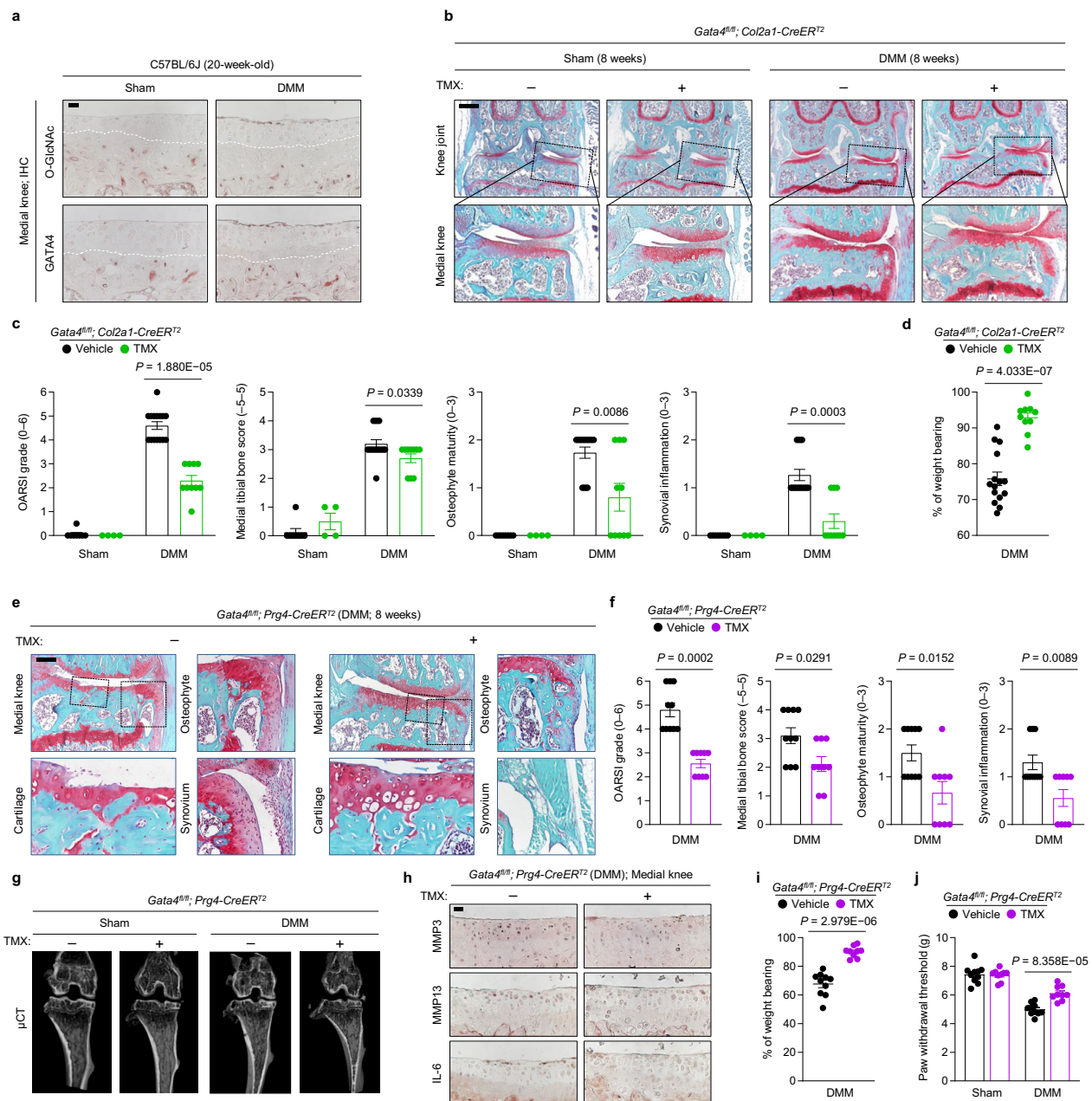
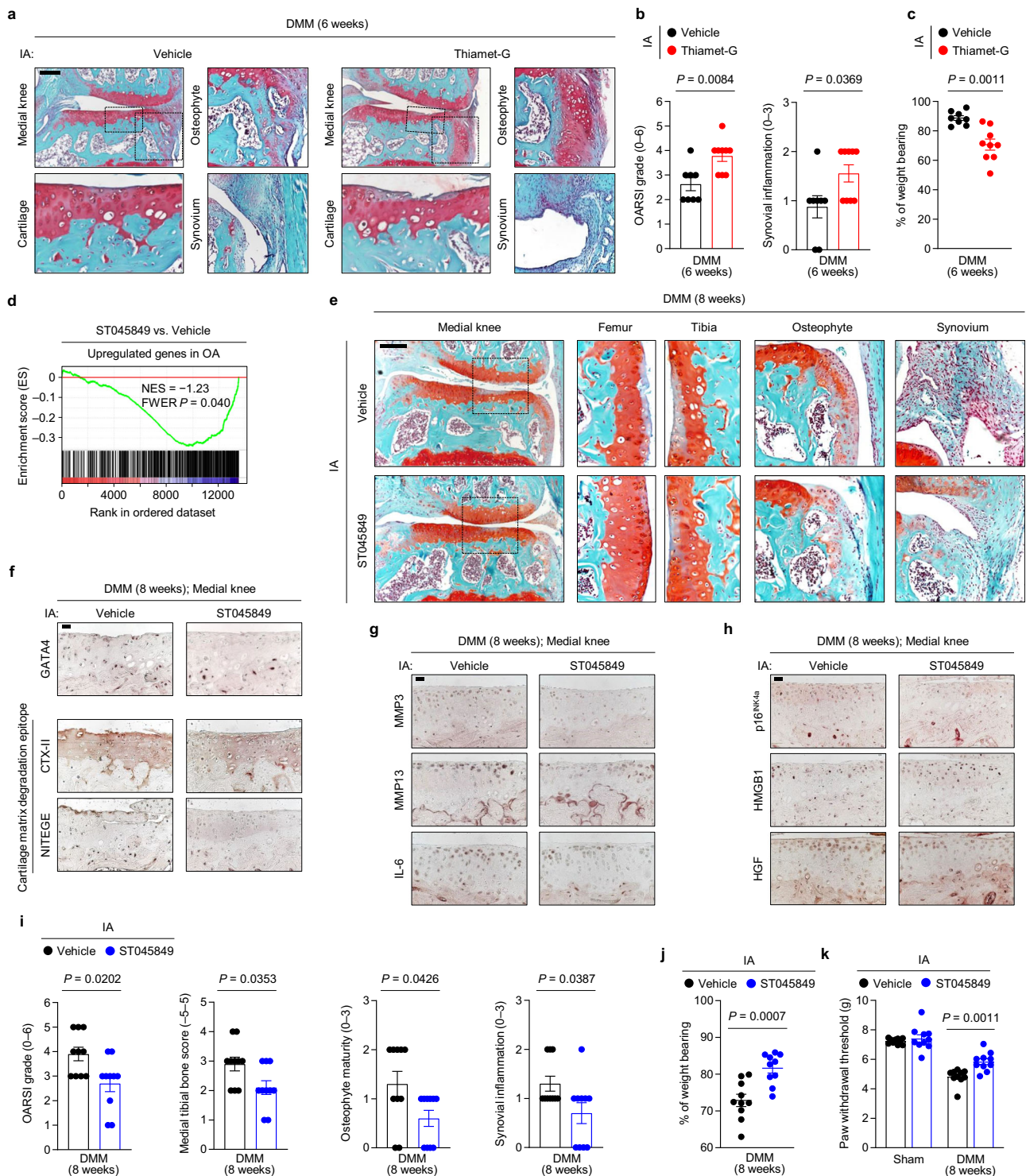


Fig. 4 | The topical deletion of *Gata4* in the superficial zone of the cartilage abolishes SASP and OA development in mice. **a** Immunohistochemistry of O-GlcNAc and GATA4 in the superficial layer of the articular cartilage from 20-week-old mouse knee joints ($n = 3$). **b** Thirteen-week-old *Gata4^{fl/fl}; Col2a1-CreER²* mice injected with vehicle or TMX received sham or DMM surgery. Joint sections were stained with safranin O, fast green, and hematoxylin, with insets magnified in the bottom row. **c** Cartilage destruction, subchondral bone sclerosis, osteophyte formation, and synovial inflammation were scored ($n = 8, 4$ for sham; $n = 15, 10$ for DMM). **d** The percentage of weight placed on the DMM-operated limb versus the contralateral limb of *Gata4^{fl/fl}; Col2a1-CreER²* mice injected with vehicle or TMX, determined using a static weight bearing test ($n = 15, 10$ respectively). **e** Thirteen-week-old *Gata4^{fl/fl}; Prg4-CreER²* mice injected with vehicle or TMX received DMM surgery. Joint sections were stained with safranin O, fast green, and hematoxylin, with insets magnified below and on the right. **f** Cartilage destruction, subchondral

bone sclerosis, osteophyte formation, and synovial inflammation were scored ($n = 10, 9$ respectively). **g** Representative μ CT images of sham- or DMM-operated *Gata4^{fl/fl}; Prg4-CreER²* mice injected with vehicle or TMX. **h** Immunohistochemistry of MMP3, MMP13, and IL-6 in cartilage sections from DMM-operated *Gata4^{fl/fl}; Prg4-CreER²* mice injected with vehicle or TMX ($n = 3$). **i** The percentage of weight placed on the DMM-operated limb versus the contralateral limb of *Gata4^{fl/fl}; Prg4-CreER²* mice injected with vehicle or TMX, determined using a static weight bearing test ($n = 10, 9$ respectively). **j** Electronic Von Frey test in the ipsilateral hindpaw of sham- or DMM-operated *Gata4^{fl/fl}; Prg4-CreER²* mice injected with vehicle or TMX ($n = 10, 9$ for sham; $n = 10, 9$ for DMM). Scale bars: **a, h**, 25 μ m, **b**, 500 μ m, **e**, 200 μ m. **c, d, f, i, j** Data represent means \pm s.e.m. *P* values are from Kruskal–Wallis test followed by two-tailed Mann–Whitney *U* test (**c**), two-tailed *t* test (**d, i, j**), or Mann–Whitney *U* test (**f**). Source data are provided as a Source Data file.

post-traumatic OA in mice (Fig. 4 and Supplementary Fig. 7). Thus, we next questioned whether controlling the extent of O-GlcNAcylation in the joints influences the progression of OA in vivo. First, we investigated whether the pharmacological inhibition of OGA to increase O-GlcNAcylation affects the progression of post-traumatic OA in mice.

Intra-articular (IA) injection of thiamet-G caused an early onset of OA phenotypes, including cartilage degeneration, subchondral bone sclerosis, osteophyte maturation, and synovial inflammation (Fig. 5a, b and Supplementary Fig. 8a). Consistently, treatment with thiamet-G significantly aggravated OA-associated pain assessed by measuring



weight imbalance and mechanical allodynia in DMM-operated mice (Fig. 5c and Supplementary Fig. 8b).

By contrast, following treatment with the OGT inhibitor ST045849, the transcriptomes of senescent chondrocytes (Supplementary Fig. 8c) were negatively enriched with “genes upregulated in OA patients” (Fig. 5d and Supplementary Fig. 8d, e). To test its potential therapeutic effect in treating OA, we loaded ST045849 in an injectable hydrogel system made of ascorbyl palmitate for its controlled release in mouse knee joints²⁴. IA injection of the hydrogel-based ST045849 delivery system effectively alleviated osteoarthritic cartilage destruction (Fig. 5e), as further supported by a marked decrease in GATA4 expression and irreversible damage of collagen and

PG detected by the neopeptides of type II collagen and aggrecan, respectively (Fig. 5f). At the same time, ST045849 delivery in DMM-operated cartilage reduced the expressions of senescence markers and SASPs (Fig. 5g, h). Treatment with ST045849 also significantly suppressed the onset of other whole-joint OA manifestations, including subchondral bone sclerosis, osteophyte development, and synovitis, as well as the development of OA-associated pain (Fig. 5i-k).

Excessive glucosamine supplementation exacerbates post-traumatic OA in mice

Glucosamine, as a precursor of UDP-GlcNAc, is frequently consumed by patients with OA and aged individuals as an easily accessible

Fig. 5 | Pharmacological modulation of O-GlcNAcylation regulates GATA4 and affects post-traumatic OA. **a** Twelve-week-old WT C57BL/6J mice underwent DMM surgery followed by weekly IA injection of vehicle or thiamet-G. Joint sections were stained with safranin O, fast green, and hematoxylin, with insets magnified below and on the right. **b** Cartilage destruction and synovial inflammation were scored ($n = 8, 9$ respectively). **c** The percentage of weight placed on the DMM-operated limb versus the contralateral limb of the WT mice injected with vehicle or thiamet-G, determined using a static weight bearing test ($n = 8, 9$ respectively). **d** GSEA of the “Upregulated genes in OA”⁸¹ gene set in chondrocytes treated with bleomycin for 24 h followed by vehicle or ST045849 treatment for five days. **e** Twelve-week-old WT C57BL/6J mice received DMM surgery followed by weekly IA injection of vehicle or ST045849 using a hydrogel-based drug delivery system. Joint sections were stained with safranin O, fast green, and hematoxylin, with insets magnified on the right. **f–h** Immunohistochemistry of **(f)** GATA4 and cartilage

matrix neopeptides (C-telopeptide of type II collagen, CTX-II and aggrecan neopeptide, NITEGE), **(g)** MMP3, MMP13, IL-6, **(h)** senescence markers (p16^{INK4a} and HMGB1), and HGF in cartilage sections from DMM-operated WT mice followed by IA injection with vehicle or ST045849 ($n = 3$). **i** Cartilage destruction, subchondral bone sclerosis, osteophyte formation, and synovial inflammation were scored ($n = 10$). **j** Percentage of weight placed on the DMM-operated limb versus the contralateral limb of WT mice injected with vehicle or ST045849, determined using a static weight bearing test ($n = 10$). **k** Electronic Von Frey test in ipsilateral hindpaw of sham- or DMM-operated WT mice IA-injected with vehicle or ST045849 using a hydrogel-based drug delivery system ($n = 10$). Scale bars: **a, e**, 200 μm , **f–h**, 25 μm . **b, c, i–k** Data represent means \pm s.e.m. *P* values are from two-tailed Mann–Whitney *U* test (**b, i**), two-tailed *t* test (**c, j, k**), or one-tailed permutation test corrected for multiple comparisons with FWER (**d**). Source data are provided as a Source Data file.

supplement, with the expectation of sustaining PG contents^{25–27}. Glucosamine, entering the pathway downstream of GFPT, circumvents this rate-limiting step to consequently expedite the production of UDP-GlcNAc^{10,11,28}. Thus, elevated levels of UDP-GlcNAc caused by glucosamine uptake potentially contribute to promoting cellular O-GlcNAc modifications⁶.

Treatment with glucosamine sulfate significantly elevated global O-GlcNAcylation (Fig. 6a and Supplementary Fig. 8f), which in turn contributed to enhancing the stability of GATA4 protein (Fig. 6b). Next, we tested the effect of excessive glucosamine supplementation in DMM-induced post-traumatic OA (Fig. 6c), as this condition is dependent on GATA4 for disease progression (Fig. 4 and Supplementary Fig. 7). Glucosamine supplementation had no significant effect on the body weight of the DMM-operated mice compared to that of control mice supplemented with water (Fig. 6d). In sham-operated mice, excessive glucosamine intake alone did not cause any noticeable OA-associated phenotypes (Fig. 6e, f). However, in DMM-operated mice, glucosamine supplementation significantly exacerbated OA development, as evidenced by augmented cartilage destruction (Fig. 6e) and accelerated OA-associated bone remodeling in the subchondral trabecular bone (Fig. 6f). Substantially elevated levels of GATA4 and OA-associated catabolic secretory factors were observed in the cartilage of DMM-operated mice receiving excessive glucosamine supplementation (Fig. 6g), concomitant with the elevated production of degenerated matrix epitopes (Supplementary Fig. 8g). Excessive glucosamine supplementation not only promoted histological manifestations of OA phenotypes, such as cartilage degeneration and subchondral bone sclerosis (Fig. 6h and Supplementary Fig. 8h), but also intensified OA-associated pain, as evidenced by mechanical allodynia (Fig. 6i) and weight imbalance (Fig. 6j), during the development of post-traumatic OA in mice.

Discussion

Chondrocyte senescence is a central cellular event that causes cartilage matrix catabolism and chronic joint inflammation during OA pathogenesis. These pathological events of senescent chondrocytes are mainly mediated by the secretion of pro-inflammatory cytokines and proteases, collectively referred to as SASP. Senolytics have emerged as attractive therapeutic drugs to remove senescent chondrocytes, which serve as the source of OA catabolism. However, senescent chondrocytes may still be important for structural support of the cartilage tissue and their abrupt removal with senolytics could be detrimental, leading to atrophy, particularly in humans with a relatively sparse distribution of chondrocytes compared to that of rodents^{29,30}. Alternatively, senostatics, an approach to modulate the SASP regulatory system without perturbing the structural integrity of tissues, have been suggested as a rational paradigm to treat the pathogenesis of OA³¹.

GATA4 has recently been described as a critical transcriptional regulator that controls a stress-induced pro-inflammatory secretory

program associated with senescence¹⁹. GATA4 expression was reported to be upregulated in senescent nucleus pulposus cells, indicating its potential association with intervertebral disc degeneration³². In OA, GATA4 was implicated in mediating the senescence of fibroblast-like synoviocytes (FLS) in the synovial intimal lining; its upregulation in FLS was attributed to the METTL3-mediated m⁶A modification of *ATG7* (Ref. 33). In our study, GATA4 expression was predominantly detected in chondrocytes residing in the superficial zone of the articular cartilage, which have been documented as a cell population that primarily contributes to osteoarthritic cartilage damage³⁴. Specific GATA4 knockout in the superficial chondrocytes abolished the expression of SASPs and delayed the development of OA in mice. Therefore, it is critical to understand the regulatory mechanisms underlying GATA4 stabilization to develop senostatics for the treatment of OA.

GATA4 is regulated by selective autophagy via its specific interaction with p62, which is abolished under senescence-inducing stress conditions^{19,35}. However, the specific mechanism by which stress conditions compromises the interactions between GATA4 and p62 to result in GATA4 accumulation remains unknown. In this study, we revealed that O-GlcNAcylation serves as a stress sensor that triggers chronic inflammatory responses in chondrocytes by suppressing the selective autophagic degradation of GATA4. Specifically, we found that O-GlcNAcylation at residue S406 of GATA4 compromises its interaction with p62, which is required for the selective inclusion of GATA4 into the autophagy-mediated lysosomal degradation pathway. The resulting accumulation of GATA4 stimulates the expression of SASPs and fosters chronic inflammation. Both in human and mouse OA cartilage, the expression patterns of O-GlcNAcylation and GATA4 highly overlapped, supporting their association in the physiological context. Pharmacological inhibition of O-GlcNAcylation abolished GATA4 expression in the articular cartilage, markedly reducing the degeneration of type II collagen and PGs and ultimately suppressing the progression of OA in a post-traumatic mouse model.

UDP-GlcNAc is the end product of the hexosamine biosynthetic pathway, which serves as a donor for the O-GlcNAcylation of target proteins. Glucosamine remains one of the most frequently consumed supplements by patients with OA and aged individuals, despite its controversial clinical trial outcomes^{25,27}. Glucosamine has been shown to enhance the production of UDP-GlcNAc by bypassing the rate-limiting step of the hexosamine biosynthetic pathway, thereby facilitating O-GlcNAc modifications^{36,37}. In this study, we demonstrated that glucosamine enhances O-GlcNAcylation and GATA4 stability in chondrocytes. Excessive glucosamine supplementation exacerbated stress-induced senescence phenotypes, thereby promoting post-traumatic OA in mice. Thus, our study proposes a caveat that excessive glucosamine consumption may need to be considered cautiously in individuals experiencing joint instability. Hyperglycemia has also been associated with upregulated UDP-GlcNAc production and O-GlcNAc

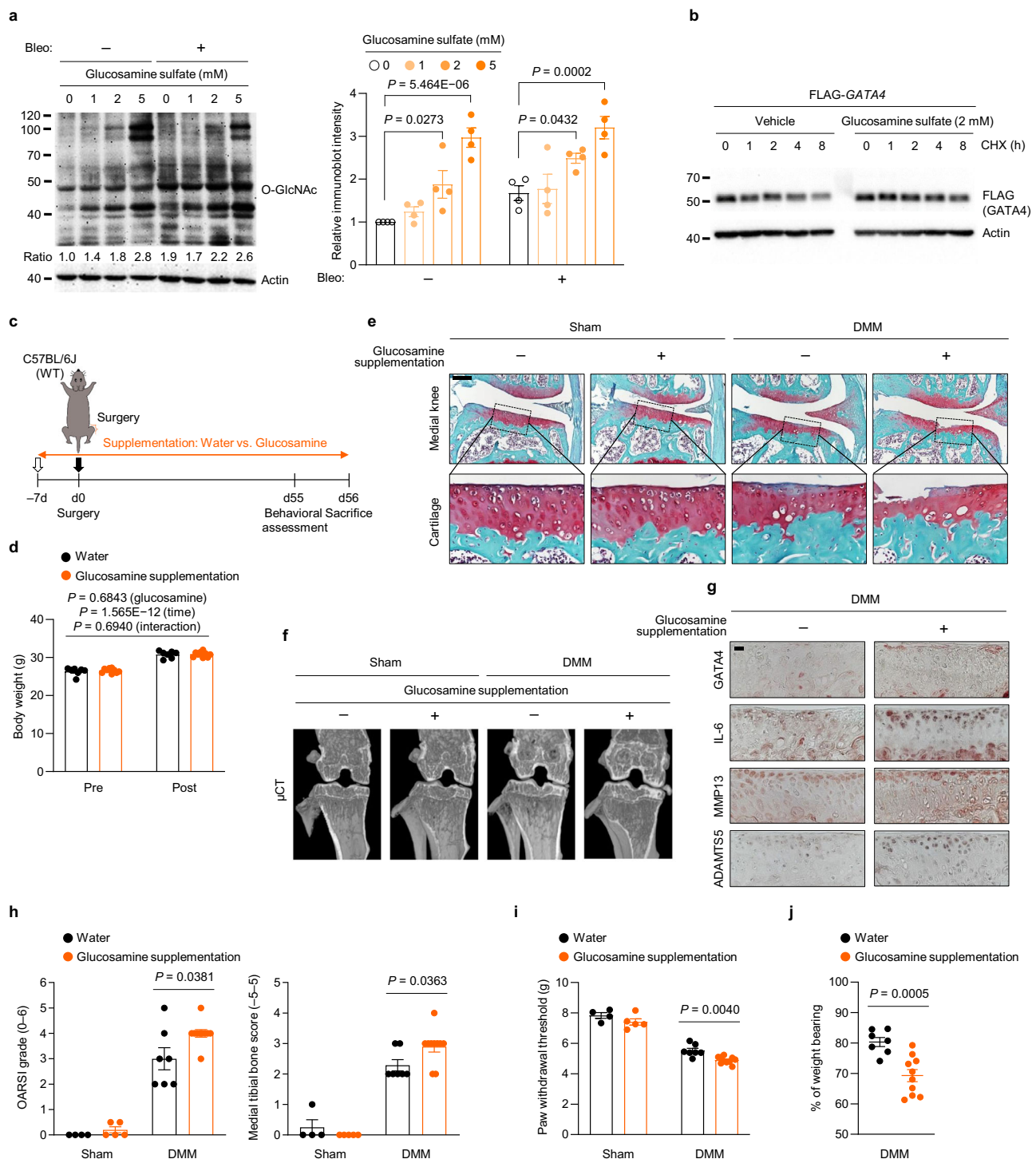


Fig. 6 | Excessive glucosamine supplementation enhances O-GlcNAcylation and GATA4 stability, aggravating post-traumatic OA in mice. a Western blot of global protein O-GlcNAcylation in primary mouse chondrocytes treated with or without bleomycin for 24 h, followed by varying doses of glucosamine sulfate for 72 h (left) and quantification of O-GlcNAcylation levels (right) ($n = 4$). **b** CHX chase analysis in HEK293T-FLAG-GATA4 treated with vehicle or glucosamine sulfate (2 mM) ($n = 3$). **c** Schematic illustration of dietary glucosamine sulfate supplementation in the post-traumatic OA model of WT mice. Twelve-week-old WT C57BL/6J mice were provided with drinking water with or without glucosamine sulfate (5 mg/mL), starting seven days prior to the sham or DMM operation. **d** Body weight of the DMM-operated mice pre- and post-supplementation of glucosamine sulfate ($n = 7, 10$ respectively). **e** Joint sections were stained with safranin O, fast green, and hematoxylin, with insets magnified in the bottom row. **f** Representative

μ CT images of sham- or DMM-operated WT mice provided with or without glucosamine sulfate. **g** Immunohistochemistry of GATA4, IL-6, MMP13, and ADAMTS5 in cartilage sections from DMM-operated WT mice provided with or without glucosamine sulfate ($n = 3$). **h** Cartilage destruction and subchondral bone sclerosis were scored ($n = 4, 5$ for sham; $n = 7, 10$ for DMM). **i** Electronic Von Frey test in the ipsilateral hindpaw of sham- or DMM-operated WT mice provided with or without glucosamine sulfate ($n = 4, 5$ for sham; $n = 7, 10$ for DMM). **j** The percentage of weight placed on the DMM-operated limb versus the contralateral limb of the mice, determined using a static weight bearing test ($n = 7, 10$ respectively). Scale bars: **e**, 200 μ m, **g**, 25 μ m. **a, d, h–j** Data represent means \pm s.e.m. P values are from two-way ANOVA followed by Dunnett's post-hoc test (**a**), two-way ANOVA followed by Bonferroni post-hoc test (**d**), two-tailed Mann-Whitney U test (**h**), or two-tailed t test (**i, j**). Source data are provided as a Source Data file.

modification^{10,38}. Our findings suggest that the hyperglycemia-induced O-GlcNAcylation could partially account for the well-established association between OA and T2DM^{39,40}. Given the mechanistic connection between O-GlcNAcylation and senescence-associated chronic inflammation, a comprehensive clinical assessment of the impact of glucosamine supplementation and blood sugar levels on OA pathogenesis is warranted for further epidemiological investigation.

We elucidate that the compartmentalization of UDP-GlcNAc serves as a key mechanism to control O-GlcNAcylation. The redirection of UDP-GlcNAc flux from secretory organelles to the cytosol is closely linked with the pathological shift in chondrocyte secretory pathways. Senescent chondrocytes cease the secretion of GAG-rich PGs, corresponding with a reduced demand for UDP-GlcNAc in the ER and Golgi apparatus, instead shifting toward the secretion of inflammatory factors. This rerouting of UDP-GlcNAc flux appears to be orchestrated by a collective reduction in the expression of members of the SLC35 transporter family, whose deficiencies are previously linked to impaired cartilage and skeletal development in mammals^{41,42}. Furthermore, senescence-driven upregulation of miR-204, resulting in the downregulation of SLC35B4 and SLC35D1, has been implicated in the diminished PG synthesis observed during OA development⁴.

In this study, we employed two different chemical agents—doxorubicin and bleomycin—to induce cellular senescence. While both are well-established senescence inducers, their distinct mechanisms of action may result in different senescent phenotypes across cell types. Doxorubicin induces DNA double-strand breaks by inhibiting topoisomerase II during the S-phase of the cell cycle, leading to replication stress and DNA damage accumulation⁴³, which ultimately trigger senescence. In contrast, bleomycin promotes senescence by generating ROS, resulting in lipid peroxidation and both single- and double-strand breaks⁴⁴. Despite these mechanistic differences, we observed that both doxorubicin and bleomycin elicited similar senescence-associated cellular responses in mouse chondrocytes, including irreversible DNA damage, cell cycle arrest, and inflammation. Nonetheless, it is important to note that the distinct damage induction mechanisms of doxorubicin and bleomycin may influence the kinetics and phenotypes of senescence.

The regulatory mechanisms of O-GlcNAcylation and its implications in OA have been investigated in previous studies. Differential regulation of various isoforms of OGT and OGA has been observed in OA cartilage⁴⁵. Specifically, nucleocytoplasmic and mitochondrial OGT are downregulated, while short OGT is upregulated in OA compared to healthy cartilage. Conversely, the full-length isoform of OGA is decreased, whereas the short isoform is increased in OA cartilage. Systemic administration of thiamet-G, which enhances global O-GlcNAcylation, led to increased hypertrophic maturation in adolescent mice, highlighting a potential link between O-GlcNAcylation and hypertrophic differentiation in chondrogenic stem/progenitor cells⁴⁶. In pathological conditions like OA, chondrocyte hypertrophy may be recapitulated, accompanied by the expression of type X collagen and MMP13⁴⁷. While we cannot entirely rule out the possibility that O-GlcNAcylation contributes to OA progression by influencing hypertrophic differentiation in chondrogenic progenitor cells, our findings suggest that O-GlcNAcylation is primarily localized in the superficial layers of cartilage, where chondrocytes experience the highest mechanical stress. It should be noted, however, that O-GlcNAcylation is highly dynamic and tissue-specific, playing roles in both protective and detrimental cellular processes. Its effects on disease progression may depend on quantitative factors, such as the duration and extent of modification, as well as the surrounding pathophysiological context^{10,11,48}.

Potential limitations of our study include the lack of precision in assessing site-specific O-GlcNAcylation of GATA4. To more accurately determine whether O-GlcNAcylation of endogenous GATA4 is specifically elevated under OA-relevant conditions, it would be crucial to

develop an antibody that specifically targets the O-GlcNAcylated form of GATA4. Recent advancements in site-specific O-GlcNAc antibodies⁴⁹ may provide valuable tools for this purpose. In this study, we used male mice due to their higher susceptibility to OA, influenced by sex hormones^{50–52}. However, human cartilage samples were obtained from female participants, reflecting the higher prevalence of OA in women⁵³. Future investigations should assess whether our findings are consistent across both sexes or account for sex-specific differences, particularly in relation to the influence of sex hormones. Regarding therapeutic strategies, it is critical to target GATA4-specific O-GlcNAcylation rather than global O-GlcNAcylation, as broad inhibition could lead to cytotoxicity. A promising direction for future research would be developing strategies that specifically disrupt GATA4 O-GlcNAcylation, by targeting protein-protein interactions between OGT and GATA4. Finally, the amount of glucosamine fed to the mice in our study was significantly higher, corresponding to a daily intake of 5.8 g for a 60 kg adult human, based on body surface area-equivalent dose calculations between the two species⁵⁴. This was done to explore the effects of excessive O-GlcNAc precursor on SASP expression under joint mechanical instability, not to test the nutritional effect of glucosamine on OA. The effects of glucosamine supplementation on OA progression should be evaluated with careful consideration of factors such as timing, dosage, route of administration, and formulation of glucosamine, combined with the pathophysiological context^{48,55,56}. The effect of glucosamine on OA may manifest through its linked influence on other diseases associated with OA, such as CVD⁴⁸.

Several animal studies have investigated the potential effects of glucosamine intake in delaying aging and reducing the risk of aging-associated diseases. D-glucosamine supplementation was shown to extend the lifespan of aged mice by suppressing glycolysis⁵⁷. Chemical agents that enhance O-GlcNAcylation, such as PUGNAc, have demonstrated joint protection following mechanical trauma, increasing type II collagen biosynthesis and reducing catabolic factors⁵⁸. However, high doses of glucosamine were found to decrease cell proliferation⁵⁹ and cause cytotoxic effects in chondrocytes⁵⁸, highlighting that the dosage of glucosamine can differentially impact chondrocyte physiology. Similarly, while the efficacy of glucosamine supplementation in OA has been investigated for decades, clinical outcomes remain inconsistent, even between major trials such as the NIH-sponsored Glucosamine/Chondroitin Arthritis Intervention Trial (GAIT)⁶⁰ and the Glucosamine Unum In Die (once-a-day) Efficacy (GUIDE) trial⁶¹.

Taken together, we have demonstrated the critical role of O-GlcNAcylation in pathologically transitioning the secretory programs of chondrocytes during OA development. The stress-induced O-GlcNAcylation of GATA4 enhances senescence-associated chronic inflammation and OA pathogenesis. Thus, targeting stress-induced O-GlcNAcylation of GATA4 may offer a promising senostatic strategy for managing senescence-associated chronic inflammation in OA.

Methods

Collection of human cartilage tissue samples

Human OA articular cartilage specimens were acquired from 10 patients with OA undergoing total knee arthroplasty (TKA) at the SNU Boramae Medical Center. The Institutional Review Board (IRB) of the SNU Boramae Medical Center approved the collection of human biological materials (IRB No. 30-2017-48) and the IRB of Seoul National University approved the use of these materials (IRB No. E1803/003-009). Written informed consent was obtained from all patients prior to the TKA surgical procedures. Patient characteristics including sex, age, height, weight, and BMI are summarized in range in Supplementary Table 3. We only used samples obtained from female patients. Human cartilage tissue sections were stained with Alcian blue and graded according to the Osteoarthritis Research Society International (OARS) grading system⁶².

Mice

Gata4^{fl/fl}, *Col2a1-CreER^{T2}*, and *Prg4-CreER^{T2}* mouse lines were obtained from The Jackson Laboratory and backcrossed with the C57BL/6J mouse line at least six times. To establish *Gata4* knockout mouse lines, *Gata4^{fl/fl}* mice were crossed with *Col2a1-CreER^{T2}* (for the conditional knockout in total chondrocytes) or *Prg4-CreER^{T2}* (for the conditional knockout in superficial chondrocytes) mouse lines. To establish the post-traumatic OA model in *Gata4* knockout mouse lines, 12-week-old male *Gata4^{fl/fl}*; *Col2a1-CreER^{T2}*, or *Gata4^{fl/fl}*; *Prg4-CreER^{T2}* mice were intra-peritoneally injected daily with 80 µg/g body weight of TMX (Sigma Aldrich, T5648) dissolved in corn oil (Sigma Aldrich, C8267) vehicle for five days. Twelve-week-old male wild-type (WT) C57BL/6J mice (Dae-han-Biolink Co.) were used for studies involving IA injection of thiamet-G or ST045849 and excessive glucosamine supplementation via drinking water.

Experimental OA in mice

All animal experiments were approved by the Institutional Animal Care and Use Committee of SNU (IACUC No. SNU-180109-1, SNU-190105-1, SNU-190919-6, SNU-210113-4). The design, analysis, and reporting of animal experiments were conducted according to the Animals in Research: Reporting of In Vivo Experiments Guidelines (<https://www.nc3rs.org.uk/arrive-guidelines>). The mice were housed in a specific pathogen-free laboratory animal facility at SNU. The animals were maintained under constant temperature (21–23 °C) and humidity (50–65%) with controlled light-dark cycles (12:12 h) and fed standard laboratory chow *ad libitum*. Glucosamine sulfate supplementation was performed by supplying mice with glucosamine sulfate potassium chloride (LKT Laboratories, G4581) dissolved in drinking water at a concentration of 5 mg/mL, aiming an estimated daily intake of 30 mg. This amount corresponds to 5.8 g daily intake in 60 kg adult human, considering the body surface area-based equivalent dose calculation between the two species⁵⁴. Post-traumatic OA was induced by DMM surgery⁶³ in 12-week-old (WT C57BL/6J) except for the excessive glucosamine supplementation experiment) or 13-week-old (*Gata4^{fl/fl}*, *Gata4^{fl/fl}*; *Col2a1-CreER^{T2}*, *Gata4^{fl/fl}*; *Prg4-CreER^{T2}*, or WT C57BL/6J) for the excessive glucosamine supplementation experiment) mice; mice of the same age who underwent sham surgery served as controls. The mice were sacrificed six or eight weeks after the sham or DMM operation. The animal experimental period is indicated in each experiment. For IA injection of OGA inhibitor for maintenance of O-GlcNAcylated status, vehicle or 20 nmol thiamet-G (Sigma Aldrich, SML0244) in 10 µL of phosphate-buffered saline (PBS) was injected intra-articularly every week in sham- or DMM-operated WT mice for six weeks. For the controlled release of the OGT inhibitor to reduce O-GlcNAcylation, a hydrogel containing dimethyl sulfoxide (DMSO; Sigma Aldrich, 276855) or 2 nmol ST045849 (Tim Tec, ST045849) was injected intra-articularly every week in the knee joints of sham- or DMM-operated WT mice for eight weeks. Hydrogels (final concentration: 4% w/v) were prepared by dissolving 6-O-palmitoyl-L-ascorbic acid (Sigma Aldrich, 76183) with or without ST045849 in DMSO, and mixing with sterilized distilled water²⁴. The hydrogels were 1:1 diluted in PBS prior to the injection. The degree of cartilage destruction and OA-associated phenotypes in the knee joints was evaluated using safranin O staining and scored according to the OARSI grading system⁶⁴.

Histological and immunohistochemical analyses

Human OA cartilage specimens were fixed in 4% paraformaldehyde (PFA), dehydrated in an increasing concentration gradient of ethanol, and incubated with xylene. The samples were embedded in paraffin and 7-µm thick sections were obtained. OA-affected cartilage samples were acquired from the tibial plateau, and relatively undamaged regions from the lateral side of the tibial plateau or relatively intact regions from the femoral condyles were used as controls. For

histological staining, the sections were deparaffinized in xylene, hydrated in a decreasing concentration gradient of ethanol, and used for Alcian blue, immunofluorescence, or immunohistochemical staining. Knee joint tissues collected from the post-traumatic OA mouse model and their respective controls were fixed with 4% PFA, decalcified in 0.5 M EDTA (pH 7.4), dehydrated in an increasing concentration gradient of ethanol, and incubated in xylene. The samples were embedded in paraffin and 5-µm thick sections were obtained. For histological staining, paraffin-embedded tissue sections were deparaffinized in xylene, hydrated in a decreasing concentration gradient of ethanol, and stained with safranin O or used for immunohistochemical staining. A comprehensive histological assessment of whole-joint tissues was performed by two orthopedic pathologists at the SNU Boramae Medical Center with extensive experience in evaluating human and mouse OA. The sections were reviewed by three additional pathologists, and at least 90% agreement was achieved for the histological grades. The observers were blinded to the cartilage tissue region of the human biological materials and the genotype, injection, or surgical condition of the mice. Images of the sections were randomized to avoid observer bias. To assess OA in mice, cartilage destruction was assessed using safranin O staining and scored in the medial tibial plateau using the OARSI grading system (0–6) (Ref. 64). Medial tibial bone sclerosis (score –5 to 5) was scored by measuring the subchondral trabecular bone to bone marrow ratio². Osteophyte maturity (grade 0–3) was graded by examining the anteromedial tibia^{65,66}. Synovial inflammation was scored on an arbitrary scale (0–3) depending on the density of the infiltrating inflammatory cells, synovial hyperplasia, and pannus invasion⁶⁷. Primary antibodies used for immunohistochemical staining were as follows: O-GlcNAc (clone RL2, Abcam, ab2739, 1:50–100), p16^{INK4a} (Proteintech, 10883-1-AP, 1:100; against human p16^{INK4a}), GATA4 (clone G-4, Santa Cruz, sc-25310, 1:50–100), IL-6 (clone 1, Santa Cruz, sc-130326, 1:50–100), MMP3 (clone EP1186Y, Abcam, ab52915, 1:50–100), MMP13 (EP1263Y, Abcam, ab51072, 1:50–100), p16^{INK4a} (clone EPR20418, Abcam, ab211542, 1:50–100; against mouse p16^{INK4a}), HMGB1 (Abcam, ab18256, 1:100), HGF (Novus, AF2207, 1:50), CTX-II (Novus, NBP2-59386, 1:100), NITEGE (clone BC-13, MD Bioproducts, 1042003, 1:100), and ADAMTSS (Abcam, ab41037, 1:100). Secondary antibodies used for immunohistochemical staining were as follows: donkey anti-mouse immunoglobulin G (IgG) (H&L) conjugated with biotin-SP (Jackson ImmunoResearch, 715-065-150, 1:200), donkey anti-rabbit IgG (H&L) conjugated with biotin-SP (Jackson ImmunoResearch, 711-065-152, 1:200), and donkey anti-goat IgG (H&L) conjugated with biotin-SP (Jackson ImmunoResearch, 705-065-147, 1:200).

Immunofluorescence

For immunofluorescence studies of human OA cartilage sections, sections of undamaged and damaged cartilage tissues were deparaffinized in xylene and hydrated in a decreasing concentration gradient of ethanol. Antigen retrieval was performed using an antigen retrieval solution (10 mM Tris-HCl, pH 9.0, 1 mM EDTA) at 60 °C for 1 h. Tissues were blocked with 10% normal goat serum (Sigma Aldrich, S26) in PBS for 10 min and incubated with primary antibodies against O-GlcNAc (clone RL2, Abcam, ab2739, 1:100), p16^{INK4a} (Proteintech, 10883-1-AP, 1:100), GATA4 (Proteintech, 19530-1-AP, 1:100), normal mouse IgG (Santa Cruz, sc-2025), and normal rabbit IgG (Cell Signaling Technology, 2729S). The tissues were washed three times with PBS and incubated with donkey anti-rabbit IgG (H&L) conjugated with Alexa Fluor 488 (ThermoFisher Scientific, A-21206, 1:200) and donkey anti-mouse IgG (H&L) conjugated with Alexa Fluor 594 (ThermoFisher Scientific, A-21203, 1:200). For immunofluorescence staining of primary culture of mouse chondrocytes, the cultured cells were fixed in 4% PFA for 15 min, permeabilized with 0.1% Triton X-100 in PBS for 10 min, and blocked with 10% normal goat serum in PBS for 1 h. The cells were incubated with primary antibodies against γ-H2AX (clone

Ser 139, Santa Cruz, sc-517348, 1:400) and normal mouse IgG (Santa Cruz, sc-2025). The cells were washed three times with PBS and incubated with rabbit anti-mouse IgG+IgM (H&L) conjugated with Alexa Fluor 488 (Jackson ImmunoResearch, 315-485-044, 1:200). After antibody treatment, the nuclei were stained with DAPI. Stained cartilage tissues and chondrocytes were mounted using ProLong Gold Antifade (ThermoFisher Scientific, P10144). The mounted slides were imaged using the EVOS FL Cell Imaging System (ThermoFisher Scientific).

Static weight bearing

The weight distribution of the sham- or DMM-operated hindlimbs and their contralateral hindlimbs was measured using the Incapacitance Meter for mice/rats (IITC Life Science, 600MR) one day prior to sacrifice. For acclimatization, mice were trained to walk into and remain in the chamber at least three times before measurement. Adaptation was performed until the mice remained stationary and did not lean against either side of the chamber. Before the measurement, each hindlimb was positioned on each recording pad of the device. The weight placed on each recording pad was measured over 1 s for at least three independent trials, and the mean value is presented. Data are presented as a percentage of the weight placed on the DMM-operated ipsilateral limb versus that on the non-surgical contralateral limb. Observers were blinded to the genotype, injection, and surgical conditions of the mice.

Electronic Von Frey test

Mechanical allodynia was measured by the Von Frey test using the Dynamic Plantar Aesthesiometer for Mechanical Stimulation (Ugo Basile) one day prior to sacrifice. Mice were placed on the metal grid floor of the device and adaptation was performed until they remained stationary for at least 15 min. When the mice stopped exploratory behavior, mechanical allodynia was tested by touching the plantar surface of the hind paw of the surgically operated limb with an electronic Von Frey filament in an ascending force at a ratio of 1.33 g/s. When the paws of the mice were withdrawn, the device automatically stopped applying force and recorded the force applied at the time of withdrawal. At least three response times were recorded per mouse and the mean value is presented as a measure of mechanical allodynia.

μ CT analysis

Anesthetized mice were scanned with an in vivo Micro-CT Scanner (Bruker, Skyscan 1276) one day prior to sacrifice. Sham- or DMM-operated hindlimbs were fixed and scanned at 0.4° for 515 scans. Scans were obtained with a setting of 70 kV X-ray source voltage, 57 μ A current, and composite X-ray filter of 0.5-mm aluminum, and images were produced at a resolution of 20 μ m pixel size. The images were reconstructed using NRecon software v1.7.3 (Bruker), and three-dimensional reconstruction of the μ CT image sets was conducted using CTVox software v3.3.0 (Bruker).

Cell culture and treatments

For the primary culture of human articular chondrocytes, the cells were isolated from the femoral condyles and tibial plateaus of human cartilage specimens collected from female patients with OA undergoing TKA⁶⁸. Cartilage tissues were dissected from the bone and treated with 0.2% pronase (Roche, 11459643001) in Dulbecco's modified Eagle's medium (DMEM)/F-12 containing 100 U/mL penicillin, 100 μ g/mL streptomycin, and 250 ng/mL amphotericin B at 37 °C for 30 min, under continuous stirring with a magnetic bar. The tissues were then digested with 0.025% collagenase (Sigma Aldrich, C6885) in DMEM/F-12 containing 5% fetal bovine serum (FBS; Gibco, 26140079), 100 U/mL penicillin, 100 μ g/mL streptomycin, and 250 ng/mL amphotericin B at 37 °C for 16–24 h with constant stirring. Human

chondrocytes were maintained in DMEM/F-12 supplemented with 10% FBS, 100 U/mL penicillin, 100 μ g/mL streptomycin, and 250 ng/mL amphotericin B. Cells were treated as indicated in each experiment at passage 1 (P1). For the primary culture of mouse articular chondrocytes, the cells were isolated from the femoral condyles and tibial plateaus of 5-day-old ICR mice of both male and female littermates⁶⁹. Joint tissues were dissected from the knee of mice and digested with 0.2% collagenase and 0.05% trypsin-EDTA in DMEM containing 100 U/mL penicillin and 100 μ g/mL streptomycin at 37 °C for 2–2.5 h. Cartilage tissues were then isolated and digested with 0.2% collagenase at 37 °C for 2–2.5 h. Mouse chondrocytes were maintained in DMEM supplemented with 10% FBS, 100 U/mL penicillin, and 100 μ g/mL streptomycin. Two days after seeding, cells were treated as indicated in each experiment. Cultured human and mouse chondrocytes were maintained in a humidified 37 °C, 5% CO₂, and 3% O₂ atmosphere^{70–72}. Human chondrocyte cell line C28/I2 (Merck, SCC043) was maintained in DMEM/F-12 supplemented with 10% FBS, 15 mM HEPES, 100 U/mL penicillin, and 100 μ g/mL streptomycin in a humidified 37 °C and 5% CO₂ atmosphere⁷³. HEK293T (ATCC, CRL-3216) cells were maintained in DMEM supplemented with 10% FBS, 100 U/mL penicillin, and 100 μ g/mL streptomycin in a humidified 37 °C and 5% CO₂ atmosphere. For doxorubicin-induced cellular senescence in the primary culture of human articular chondrocytes, cells were maintained for five days at passage 0 (P0), trypsinized, and seeded into new dishes. Two days after seeding, human chondrocytes were treated with doxorubicin at P1. After seeding and allowing 72 h for stable adhesion, cellular senescence was induced by treating 1.5×10^5 primary cultured human chondrocytes (in a 35 mm culture dish) with 2 ml of growth medium containing 0, 0.2, 0.5, or 1.0 μ M of doxorubicin (Cayman, 15007) for 14 days. To prevent nutrient deprivation while maintaining the paracrine effects of SASPs, we replaced 1 ml of the medium with fresh medium containing either 2 μ L of vehicle (PBS) or an equivalent volume of doxorubicin stock solutions (prediluted to 0.1, 0.25, and 0.5 mM) every two days. For bleomycin-induced cellular senescence in the primary culture of mouse articular chondrocytes, the cells were treated with hyaluronidase type I-S (4 U/mL; Sigma Aldrich, H3506) for 4 h, vehicle or 50 μ g/mL of bleomycin for the next 24 h, and harvested after five days. For IR-induced senescence, cells were irradiated with gamma rays at a dose rate of 4 Gy/min using GC 3000 Elan irradiator (MDS Nordion). As an oxidative stress-induced senescence model, the mouse chondrocytes were treated with vehicle or 100 μ M of H₂O₂ (Sigma Aldrich, H3410) for five days. For glucosamine sulfate treatment in mouse chondrocytes, the cells were treated with or without 50 μ g/mL of bleomycin for 24 h, and indicated doses of glucosamine sulfate for the next 72 h.

Inhibition of GATA4 in senescent chondrocytes using small interfering RNA (siRNA) transfection and small-molecule inhibitor treatment

For bleomycin treatment in mouse chondrocytes, two days after seeding, the cells were treated with hyaluronidase type I-S (4 U/mL) for 4 h and vehicle or 50 μ g/mL of bleomycin for the next 24 h. For siRNA transfection in bleomycin-treated mouse chondrocytes, transfection was performed using METAFECTENE PRO (Biont, T040) and 50 nM of siRNA (a mixture of two siRNA sequences for *Gata4* knockdown) according to the manufacturer's instructions. After 12 h of transfection, the cells were further incubated in a fresh medium for 120 h. All siRNAs, including negative control siRNA (si-NC), used for RNA interference in this study were purchased from Bioneer and are listed in Supplementary Table 4. For 2-(1,3-benzodioxol-5-ylmethyl)butanedioic acid (NSC140905; AA Blocks, AA01FPKH) treatment in bleomycin-treated mouse chondrocytes, vehicle (DMSO) or 50 μ M of NSC140905 was treated for 120 h. Fresh medium was supplemented every 48 h.

Immunoblotting

After the treatments, the cells were washed twice with PBS and lysed with RIPA buffer containing a protease inhibitor (Sigma Aldrich, S8820). For overexpression-based experiments, HEK293T cells were transfected with a doxycycline (Doxy)-inducible GATA4 plasmid (Fig. 3d) or a TK promoter-driven FLAG-tagged GATA4 (WT, S212A, S406A) plasmid (Fig. 3f, j) using a polyethylenimine (PEI) polymer. After 6 or 24 h of transfection, the medium was treated and maintained as described in each figure legend. Next, 10 to 15 μg of cell lysates were fractionated by SDS-PAGE and transferred onto a nitrocellulose membrane (GE Healthcare, 10600002). Membranes were blocked with 3% nonfat milk or 2% bovine serum albumin (BSA) in Tris-buffered saline (TBS) containing 0.1% Tween 20 for 1 h and incubated with primary antibodies at 4 °C overnight. After removing unbound antibodies by washing three times, the membranes were incubated with secondary antibodies. Immunoreactive protein bands were detected using SuperSignal West Dura Extended Duration Substrate (ThermoFisher Scientific, 34075) with iBright FL1000 (ThermoFisher Scientific). Primary antibodies used for immunoblotting were as follows: O-GlcNAc (clone RL2, Abcam, ab2739, 1:1000–3000), p16^{INK4a} (Proteintech, 10883-1-AP, 1:1000), GATA4 (clone G-4, Santa Cruz, sc-25310, 1:100), MMP3 (clone EP1186Y, Abcam, ab52915, 1:1000), MMP13 (EP1263Y, Abcam, ab51072, 1:500), IL-6 (clone 1, Santa Cruz, sc-130326, 1:1000), HA (Abcam, ab9110, 1:2000), FLAG (clone M2, Sigma Aldrich, F3165, 1:4000), vinculin (clone E1E9V, Cell Signaling Technology, 13901, 1:2000–5000), and actin (clone C-11, Santa Cruz, sc-1615, 1:2000–4000). Secondary antibodies used for immunoblotting were as follows: goat anti-rabbit IgG (H&L) conjugated with horseradish peroxidase (HRP) (Jackson ImmunoResearch, 111-035-003), goat anti-mouse IgG+IgM (H&L) conjugated with HRP (Jackson ImmunoResearch, 115-035-044), and donkey anti-goat IgG conjugated with HRP (Santa Cruz, sc-2020). Protein band intensity was quantified by densitometric analysis using ImageJ software and normalized to the corresponding housekeeping protein bands.

Immunoprecipitation

For overexpression-based experiments, HEK293T cells were transfected with FLAG-tagged GATA4 and HA-tagged OGT plasmids (Fig. 3a), HA-tagged GATA4 plasmid (Fig. 3b, c), or TK promoter-driven FLAG-tagged GATA4 (WT, S406A) plasmid (Fig. 3k and Supplementary Fig. 6d) using PEI. After 6 or 24 h of transfection, the medium was treated and maintained as described in each figure legend. For the antibody-based immunoprecipitation assay, cell lysates were prepared using EBC200 buffer (50 mM Tris-HCl, pH 8.0, 200 mM NaCl, and 0.5% NP-40) containing a protease inhibitor. For the sWGA pull-down assay, NETN buffer (20 mM Tris-HCl, pH 8.0, 100 mM NaCl, 0.5% NP-40, and 1 mM EDTA) was used. Pull-down assays were performed with the indicated antibodies and Protein A/G-Sepharose beads (GE Healthcare, 17-5280-01 and 17-0618-01) or sWGA agarose beads. The bound proteins were fractionated using SDS-PAGE and transferred onto a nitrocellulose membrane. Membranes were blocked with 3% nonfat milk or 2% BSA in TBS containing 0.1% Tween 20 for 1 h and incubated with primary antibodies at 4 °C overnight. After removing unbound antibodies by washing three times, the membranes were incubated with secondary antibodies. Immunoreactive protein bands were detected using SuperSignal West Femto Maximum Sensitivity Substrate (ThermoFisher Scientific, 34094) with iBright FL1000 (ThermoFisher Scientific). The antibodies used for the pull-down assays were as follows: FLAG (clone M2, Sigma Aldrich, F3165, 0.5 μg) and HA (Abcam, ab9110, 0.5 μg). The primary antibodies used for immunoblotting were as follows: FLAG (clone M2, Sigma Aldrich, F3165, 1:4000), HA (Abcam, ab9110, 1:2000), O-GlcNAc (clone RL2, Abcam, ab2739, 1:1000), actin (clone C-11, Santa Cruz, sc-1615, 1:4000), and vinculin (clone E1E9V, Cell Signaling Technology, 13901, 1:5000). Secondary antibodies used for immunoblotting were as follows: goat anti-rabbit IgG (H&L)

conjugated with HRP (Jackson ImmunoResearch, 111-035-003), goat anti-mouse IgG+IgM (H&L) conjugated with HRP (Jackson ImmunoResearch, 115-035-044), and donkey anti-goat IgG conjugated with HRP (Santa Cruz, sc-2020).

Measurement of UDP-GlcNAc level

C28/12 cells were treated with 100 μM of DON (Sigma Aldrich, D2141) for 24 h or 100 nM of doxorubicin for four days. For treatments in the primary culture of mouse articular chondrocytes, the cells were treated with 150 μM of DON for 24 h or 50 $\mu\text{g}/\text{mL}$ of bleomycin for 24 h; the culture medium was then replaced with fresh medium and cells were incubated for five days. Following treatment, cells were washed twice with PBS and subjected to distinct cellular lysis methods tailored for their respective purposes. For the isolation of the intact ER, MinuteTM ER Enrichment Kit (Invent Biotechnologies, ER-036) was used, and the ER compartments were dissolved in MinuteTM Denaturing Protein Solubilization Reagent (Invent Biotechnologies, WA-009). For the isolation of the intact Golgi apparatus, MinuteTM Golgi Apparatus Enrichment Kit (Invent Biotechnologies, GO-037) was used, and the cis- and trans-Golgi compartments dissolved in the solubilization reagent were combined. For the fractionation of the cytosol excluding membrane-enclosed organelles, Cell Fractionation Kit - Standard (Abcam, ab109719) was used. For whole cell lysis, cells were lysed with RIPA buffer. UDP-GlcNAc was measured as follows: 50 μL of extract sample was initially added to 50 μL of acetonitrile, hydrolyzed with 50 μL of 1 M HCl at 80 °C for 20 min, and then cooled on ice. The sample was then briefly centrifuged, neutralized with 10 μL of 1 M KOH and 50 μL of 200 mM potassium tetraborate, incubated at 80 °C for 25 min, and cooled on ice. 150 μL of Ehrlich's reagent (0.67 M p-dimethylaminobenzaldehyde and 11% (v/v) HCl in acetic acid, 1:2 diluted in acetic acid before use) was added and the reaction mixture was incubated for 30 min at 37 °C. The sample was centrifuged and 200 μL of supernatant was transferred to the microtiter plate for optical density measurement at 584 nm. The nanomolar concentrations of UDP-GlcNAc were calculated using a standard curve of UDP-GlcNAc (Sigma Aldrich, U4375), normalized to the protein content determined using PierceTM BCA Protein Assay Kit (ThermoFisher Scientific, 23225), and expressed as a percentage content compared to the vehicle control⁷⁴.

sGAG assay

C28/12 cells were maintained in DMEM/F-12 supplemented with 10% FBS, 15 mM HEPES, 100 U/mL penicillin, and 100 $\mu\text{g}/\text{mL}$ streptomycin with or without 100 nM of doxorubicin for four days. Primary cultured mouse chondrocytes were treated with bleomycin for 24 h or IR (5 Gy). Cells were maintained in DMEM supplemented with 100 U/mL penicillin and 100 $\mu\text{g}/\text{mL}$ streptomycin without FBS for 5 days⁴. The cell culture medium was replaced daily and the sGAG content of the medium from the last 24 h of treatment was analyzed. The sGAG content in the culture medium was determined using a 1,9-dimethylmethylene blue dye assay by measuring the absorbance at 525 nm. The sGAG content was quantified using a standard curve determined by the range of chondroitin sulfate solutions (Tokyo Chemical Industry, C0335) and normalized using the 3-(4,5-dimethylthiazol-2-yl)-2,5-diphenyltetrazolium bromide (MTT; Goldbio, T-030-1) assay. For the MTT assay, 100 $\mu\text{g}/\text{mL}$ of PBS-based MTT solution was applied to the cell culture for 2 h, followed by washing with PBS. DMSO was applied to solubilize the precipitate and the absorbance of the solution was measured at 570 nm.

GATA reporter gene assay

HEK293T cells were transfected with GATA reporter plasmid (0.45 μg), constitutive *Renilla* luciferase plasmid (0.1 μg), and TK promoter-driven empty or HA-GATA4 overexpression plasmid (0.45 μg) using PEI. The GATA reporter gene construct contains GATA-binding

elements in the promoter region of the firefly luciferase coding sequence. After 24 h of transfection, the medium was replaced with fresh medium containing 20 μ M of thiamet-G, 20 μ M of ST045849, or an equal volume of DMSO, and the cells were incubated for 48 h. Cells were washed with PBS and lysed with passive lysis buffer. The reporter gene activity was measured using a Dual-Luciferase Assay Kit (Promega, E1910).

CHX chase analysis

For the assessment of thiamet-G effect on GATA4 stability, HEK293T cells were transfected with GATA4 overexpression plasmid (1 μ g) using PEI. After 6 h of transfection, the medium was replaced with fresh medium containing 20 μ M of thiamet-G or an equal volume of DMSO for 36 h. For the assessment of glucosamine effect on GATA4 stability, HEK293T cells were transfected with GATA4 overexpression plasmid (0.5 μ g) using PEI. After 6 h of transfection, the medium was replaced with fresh medium containing 2 mM of glucosamine sulfate or an equal volume of PBS for 36 h. Then, the cells were treated with or without 50 μ M of CHX for the indicated time before lysis. 10 μ g of cell lysates were fractionated by SDS-PAGE to analyze protein stability.

Mapping of GATA4 O-GlcNAcylation sites using electron-transfer dissociation-mass spectrometry (ETD-MS)

The eluted GATA4 sample was subjected to electrophoresis and the band corresponding to GATA4 was extracted by in-gel digestion⁷⁵. The extracted peptides were resuspended in solvent A (0.1% formic acid in water; ThermoFisher Scientific, 28905), loaded onto C18 trap column (Acclaim PepMap100, ThermoFisher Scientific, 75 μ m \times 2 cm, 100 \AA), and separated over C18 analytical column (PepMap RSLC, ThermoFisher Scientific, 75 μ m \times 15 cm, 100 \AA) with a 4–12% linear gradient of solvent B (0.1% formic acid in acetonitrile) for 50 min at a flow rate of 300 nL/min. Mass spectra were recorded using an Orbitrap Fusion Tribrid mass spectrometer (ThermoFisher Scientific) interfaced with EASY-nanoLC (Proxeon Biosystems). Raw data were processed using the Trans-Proteomic Pipeline (v4.8.0 PHILAE) and compared to a database composed of human GATA4 (P43694, UniProt) using the SEQUEST HT search engine in Proteome Discoverer 2.2 (ThermoFisher Scientific). Carbamidomethylation of cysteine (57 Da) was considered as the fixed modification, and variable modifications were set for the oxidation of methionine (16 Da) and O-GlcNAcylation of serine and threonine (203 Da).

SA- β -Gal staining

Cultured human and mouse chondrocytes were washed twice with PBS and fixed in a fixation solution containing 2% PFA and 0.2% glutaraldehyde for 5 min. Fixed cells were washed and incubated in SA- β -Gal staining solution at 37 $^{\circ}$ C for 12–16 h. After incubation, the cells were washed twice with PBS and mounted in a 50% glycerol solution. Stained cells were imaged using Eclipse Ni-U microscope (Nikon). Total cells and SA- β -Gal-positive cells were counted in three random fields per each biological replicate⁷⁶.

5-Bromo-2'-deoxyuridine (BrdU) cell proliferation assay

C28/I2 cells or primary cultured mouse chondrocytes were seeded onto coverslips placed in a culture dish. During the treatment with doxorubicin (in C28/I2 cells) or bleomycin or IR (in mouse chondrocytes), cultured cells were exposed to 10 μ M BrdU (Sigma Aldrich, B9285) for 12 h before fixation. Fixation was performed using an ethanol fixative (pH 2.0, 15 mM glycine, 70% ethanol) at -20° C for 20 min. Cells were blocked with 10% normal goat serum and 0.1% BSA in PBS for 1 h and incubated with primary antibody against BrdU (clone IIB5, Santa Cruz, sc-32323, 1:200) at 4 $^{\circ}$ C overnight. The cells were washed three times and incubated with rabbit anti-mouse IgG+IgM (H&L) conjugated with Alexa Fluor 488 (Jackson ImmunoResearch,

315-485-044, 1:200) for 1 h. After antibody treatment, the nuclei were stained with DAPI. Stained human and mouse chondrocytes were mounted using ProLong Gold Antifade. The mounted slides were imaged using EVOS M7000 Imaging System (Invitrogen).

Quantitative reverse transcription-polymerase chain reaction (qRT-PCR)

Total RNA was extracted from cells using TRI reagent (Molecular Research Center, Inc., TR 118) and reverse-transcribed using EasyScript Reverse Transcriptase (TransGen Biotech, AE101-03) and oligo(dT) primers. To quantitatively analyze mRNA transcript levels, cDNA was amplified using qRT-PCR with Power SYBR Green PCR Master Mix (ThermoFisher Scientific, 4367659) on StepOnePlus Real-Time PCR System (Applied Biosystems). The primers used for qRT-PCR are listed in Supplementary Table 4. For qRT-PCR-based quantification data comparing the effects of various treatments, we normalized the measurements from the treatment groups to those from the control groups for each biologically independent trial, using *Hprt* as an internal control. For cell-based experiments, each set of primary cultured chondrocytes was considered a biologically independent trial. We then averaged the normalized values from multiple biologically independent trials.

RNA sequencing

Mouse primary chondrocytes were treated with hyaluronidase type I-S (4 U/mL) for 4 h under serum-free condition prior to bleomycin treatment. Cells were treated with 50 μ g/mL of bleomycin or an equal volume of PBS in serum-supplemented medium for 24 h. Then, cells were washed twice with PBS and incubated in a fresh medium containing DMSO or 20 μ M of ST045849 for five days. Fresh medium was supplemented every 48 h. Three biological replicates were used for each experimental group. Total RNA was extracted using TRI reagent and 1 μ g of total RNA was converted into cDNA libraries using the TruSeq Stranded mRNA Sample Prep kit (Illumina) in accordance with the TruSeq Standard mRNA Sample Preparation Guide, Part #15031047 Rev. E. Poly-adenylated RNA was purified using magnetic beads conjugated to oligo(dT) primers. Purified mRNA was fragmented and converted into first-strand cDNA using reverse transcriptase and random hexamer primers, with the addition of actinomycin D. Second-strand cDNA was prepared by eliminating the RNA template and synthesizing complementary strand in the presence of dUTP instead of dTTP. A single A base was added to the 3' end to enable the ligation of sequencing adapters containing a single T overhang. The ligated cDNA was amplified by PCR, while the polymerase stops when it encounters a U base to render the second strand a poor template. The final cDNA libraries were analyzed for size distribution, quantified on Agilent Technologies 2100 Bioanalyzer using a DNA 1000 chip, and normalized to 2 nM for sequencing. RNA sequencing was performed using NovaSeq 6000 (Illumina). All RNA-seq procedures were performed by Macrogen. Reads were trimmed with Trimmomatic and aligned to the reference genome *Mus musculus* (GRCm38) using STAR aligner⁷⁷. Transcript assembly and abundance estimations were performed using StringTie v2.2.0 (Ref. 78). The aligned reads were assembled into known, novel, and alternative splicing transcripts, and the relative abundance of each transcript was quantified in read count using StringTie v2.2.0. Statistical significance of differential expression was determined using DESeq2 R package⁷⁹.

Bioinformatic analysis of RNA-seq data and public datasets

For GSEA, gene lists of the RNA-seq data were ranked based on FC values. GSEA software v4.2.2 (Ref. 80) was used in pre-ranked mode, with all default parameters, for the “Degradation of the extracellular matrix” (Reactome) and “Positive regulation of cytokine production involved in inflammatory response” (GOBP) gene sets. GSEA was also performed with a list of 752 (Ref. 81) and 150 (Ref. 24) genes significantly upregulated in OA as a gene set representing “Upregulated

genes in OA". The GATA4 target gene set used for GSEA was retrieved from TRANSFAC Curated Transcription Factor Targets (https://maayanlab.cloud/Harmonizome/gene_set/GATA4/TRANSFAC+Curated+Transcription+Factor+Targets). The genes used for GSEA are listed in Supplementary Tables 5–9. Normalized enrichment score (NES) and family-wise error rate (FWER)-corrected P value are presented on GSEA plots. For PCA, variance-stabilizing transformation was applied to RNA-seq data. Principal component 1 (PC1) and PC2 were calculated based on transformed expression of 500 most variable genes using scikit-learn 1.1.3 python library. Hallmark gene set analysis was conducted with DEGs using Enrichr. The top most enriched gene sets were selected based on P values calculated from Fisher's exact test. Canonical pathways analysis was performed using Ingenuity Pathway Analysis (IPA; Qiagen Inc., <https://digitalinsights.qiagen.com/IPA>)⁸². Significantly downregulated DEGs in RNA-seq data were determined by cutoff $P < 0.01$ and FC cutoff < -1 . The enrichment P values and activation z-scores of the top 20 canonical pathways analysis are presented as graphs, and the pathways are listed in Supplementary Table 2. Public transcriptome datasets for OA or OA-relevant conditions in various in vitro and in vivo models were obtained from the GEO database. Transcriptomes of human OA cartilage (GSE16464, GSE43923, GSE64394, GSE113825, GSE117999, GSE178557, and GSE186220), IL-1 β -treated chondrocytes (GSE6119, GSE104793, and GSE163080), and cartilage from various OA animal models (DMM surgery: GSE26475, GSE53857, GSE101573, and GSE143447; anterior cruciate ligament transection (ACLT) surgery: GSE110268; monoiodoacetate (MIA) injection: GSE28958) were analyzed.

Statistical analysis

All experiments were conducted with at least three independent biological replicates. For in vitro experiments, a comparison of experimental groups was performed using a parametric test based on two-tailed Student's t test, one-way analysis of variance (ANOVA) followed by Dunnett's post-hoc test, two-way ANOVA followed by Tukey's post-hoc test, or two-way ANOVA followed by Dunnett's post-hoc test. For in vivo experiments, each independent trial was conducted using an individual mouse. To determine the statistical significance, a non-parametric test based on two-tailed Mann–Whitney U test was used. Data quantified based on ordinal grading systems such as the OARSI grade and scores for subchondral bone sclerosis, osteophyte maturity, and synovial inflammation, whose data points are not continuous and do not follow a normal distribution, were analyzed using non-parametric methods. Otherwise, two-tailed Student's t test or two-way ANOVA followed by Bonferroni post-hoc test was applied. Separate statistical analyses were performed for the sham and DMM groups such that the surgical condition was not considered a variable (as in the cases described in Refs. 83–85). Statistical significance was set at $P < 0.05$. Statistical analyses were performed using IBM SPSS Statistics 25 or GraphPad Prism 10.0. All the graphs and heatmaps were plotted using GraphPad Prism 10.0. Cell cultures and animals were randomly assigned to each experimental group and all samples were evaluated in a blinded manner. The sample size n required for each group of animal studies to provide acceptable power was determined based on a power analysis calculation (Eq. 1) and the design of previous studies^{86,87}. No exclusion criteria were applied for this study.

$$n = \frac{2\sigma^2(z_{\frac{\alpha}{2}} + z_{\beta})^2}{D^2} \quad (1)$$

where $D = \hat{\mu}_{treatment} - \hat{\mu}_{control}$, σ = standard deviation, α = significance level (0.05), and $1 - \beta$ = power (0.90).

Reporting summary

Further information on research design is available in the Nature Portfolio Reporting Summary linked to this article.

Data availability

The original RNA-seq datasets generated in this study have been deposited in the GEO database under accession numbers GSE275524 and GSE281015. Transcriptome data for OA or OA-relevant conditions in various in vitro and in vivo models were obtained from the GEO database. Transcriptomes of human OA cartilage (GSE16464, GSE43923, GSE64394, GSE113825, GSE117999, GSE178557, and GSE186220), IL-1 β -treated chondrocytes (GSE6119, GSE104793, and GSE163080), and cartilage from various OA animal models (DMM surgery: GSE26475, GSE53857, GSE101573, and GSE143447; ACLT surgery: GSE110268; MIA injection: GSE28958) were analyzed. All other relevant data supporting the findings of this study are available within the article and its Supplementary Information file or from the corresponding author upon request. Source data are provided with this paper.

References

- Hunter, D. J., March, L. & Chew, M. Osteoarthritis in 2020 and beyond: a Lancet Commission. *Lancet* **396**, 1711–1712 (2020).
- Jeon, O. H. et al. Local clearance of senescent cells attenuates the development of post-traumatic osteoarthritis and creates a pro-regenerative environment. *Nat. Med.* **23**, 775–781 (2017).
- Coryell, P. R., Diekman, B. O. & Loeser, R. F. Mechanisms and therapeutic implications of cellular senescence in osteoarthritis. *Nat. Rev. Rheumatol.* **17**, 47–57 (2021).
- Kang, D. et al. Stress-activated miR-204 governs senescent phenotypes of chondrocytes to promote osteoarthritis development. *Sci Transl Med* **11**, <https://doi.org/10.1126/scitranslmed.aar6659> (2019).
- Heinegard, D. & Saxne, T. The role of the cartilage matrix in osteoarthritis. *Nat. Rev. Rheumatol.* **7**, 50–56 (2011).
- Vigetti, D. et al. Role of UDP-N-acetylglucosamine (GlcNAc) and O-GlcNAcylation of hyaluronan synthase 2 in the control of chondroitin sulfate and hyaluronan synthesis. *J. Biol. Chem.* **287**, 35544–35555 (2012).
- Qu, C. J., Jauhiainen, M., Auriola, S., Helminen, H. J. & Lammi, M. J. Effects of glucosamine sulfate on intracellular UDP-hexosamine and UDP-glucuronic acid levels in bovine primary chondrocytes. *Osteoarthr. Cartil.* **15**, 773–779 (2007).
- Banerjee, P. S., Hart, G. W. & Cho, J. W. Chemical approaches to study O-GlcNAcylation. *Chem. Soc. Rev.* **42**, 4345–4357 (2013).
- Hart, G. W. Nutrient regulation of signaling and transcription. *J. Biol. Chem.* **294**, 2211–2231 (2019).
- Bond, M. R. & Hanover, J. A. O-GlcNAc cycling: a link between metabolism and chronic disease. *Annu. Rev. Nutr.* **33**, 205–229 (2013).
- Yang, X. & Qian, K. Protein O-GlcNAcylation: emerging mechanisms and functions. *Nat. Rev. Mol. Cell Biol.* **18**, 452–465 (2017).
- Yang, W. H. et al. Modification of p53 with O-linked N-acetylglucosamine regulates p53 activity and stability. *Nat. Cell Biol.* **8**, 1074–1083 (2006).
- Buren, S. et al. Regulation of OGT by URI in Response to Glucose Confers c-MYC-Dependent Survival Mechanisms. *Cancer Cell* **30**, 290–307 (2016).
- Peng, C. et al. Regulation of the Hippo-YAP Pathway by Glucose Sensor O-GlcNAcylation. *Mol. Cell* **68**, 591–604.e595 (2017).
- Yang, X. et al. Phosphoinositide signalling links O-GlcNAc transferase to insulin resistance. *Nature* **451**, 964–969 (2008).
- Zhu-Mauldin, X., Marsh, S. A., Zou, L., Marchase, R. B. & Chatham, J. C. Modification of STIM1 by O-linked N-acetylglucosamine (O-GlcNAc) attenuates store-operated calcium entry in neonatal cardiomyocytes. *J. Biol. Chem.* **287**, 39094–39106 (2012).
- Krishnamurthy, J. et al. Ink4a/Arf expression is a biomarker of aging. *J. Clin. Investig.* **114**, 1299–1307 (2004).
- Ring, N. A. R., Valdivieso, K., Grillari, J., Redl, H. & Ogrodnik, M. The role of senescence in cellular plasticity: Lessons from regeneration

- and development and implications for age-related diseases. *Dev. Cell* **57**, 1083–1101 (2022).
19. Kang, C. et al. The DNA damage response induces inflammation and senescence by inhibiting autophagy of GATA4. *Science* **349**, aaa5612 (2015).
 20. Gillespie, M. et al. The reactome pathway knowledgebase 2022. *Nucleic Acids Res* **50**, D687–D692 (2022).
 21. Gene Ontology, C. The Gene Ontology resource: enriching a GOLD mine. *Nucleic Acids Res* **49**, D325–D334 (2021).
 22. El-Hachem, N. & Nemer, G. Identification of new GATA4-small molecule inhibitors by structure-based virtual screening. *Bioorg. Med Chem.* **19**, 1734–1742 (2011).
 23. Negroni, C. et al. GATA-4, a potential novel therapeutic target for high-grade meningioma, regulates miR-497, a potential novel circulating biomarker for high-grade meningioma. *EBioMedicine* **59**, 102941 (2020).
 24. Kim, S. et al. Tankyrase inhibition preserves osteoarthritic cartilage by coordinating cartilage matrix anabolism via effects on SOX9 PARylation. *Nat. Commun.* **10**, 4898 (2019).
 25. Runhaar, J. et al. Subgroup analyses of the effectiveness of oral glucosamine for knee and hip osteoarthritis: a systematic review and individual patient data meta-analysis from the OA trial bank. *Ann. Rheum. Dis.* **76**, 1862–1869 (2017).
 26. Ogata, T. et al. Effects of glucosamine in patients with osteoarthritis of the knee: a systematic review and meta-analysis. *Clin. Rheumatol.* **37**, 2479–2487 (2018).
 27. Fernandez-Martin, S. et al. Glucosamine and Chondroitin Sulfate: Is There Any Scientific Evidence for Their Effectiveness as Disease-Modifying Drugs in Knee Osteoarthritis Preclinical Studies?—A Systematic Review from 2000 to 2021. *Animals (Basel)* **11**, <https://doi.org/10.3390/ani11061608> (2021).
 28. Marshall, S., Nadeau, O. & Yamasaki, K. Dynamic actions of glucose and glucosamine on hexosamine biosynthesis in isolated adipocytes: differential effects on glucosamine 6-phosphate, UDP-N-acetylglucosamine, and ATP levels. *J. Biol. Chem.* **279**, 35313–35319 (2004).
 29. Collins, J. A., Diekman, B. O. & Loeser, R. F. Targeting aging for disease modification in osteoarthritis. *Curr. Opin. Rheumatol.* **30**, 101–107 (2018).
 30. Dolgin, E. Send in the senolytics. *Nat. Biotechnol.* **38**, 1371–1377 (2020).
 31. Kang, C. Senolytics and Senostatics: A Two-Pronged Approach to Target Cellular Senescence for Delaying Aging and Age-Related Diseases. *Mol. Cells* **42**, 821–827 (2019).
 32. Wang, X. H. et al. GATA4 promotes the senescence of nucleus pulposus cells via NF-kappaB pathway. *Arch. Gerontol. Geriatr.* **101**, 104676 (2022).
 33. Chen, X. et al. METTL3-mediated m(6)A modification of ATG7 regulates autophagy-GATA4 axis to promote cellular senescence and osteoarthritis progression. *Ann. Rheum. Dis.* **81**, 87–99 (2022).
 34. Zhang, M. et al. Induced superficial chondrocyte death reduces catabolic cartilage damage in murine posttraumatic osteoarthritis. *J. Clin. Invest* **126**, 2893–2902 (2016).
 35. Mancias, J. D. & Kimmelman, A. C. Mechanisms of Selective Autophagy in Normal Physiology and Cancer. *J. Mol. Biol.* **428**, 1659–1680 (2016).
 36. Slawson, C., Copeland, R. J. & Hart, G. W. O-GlcNAc signaling: a metabolic link between diabetes and cancer? *Trends Biochem Sci.* **35**, 547–555 (2010).
 37. Baudoin, L. & Issad, T. O-GlcNAcylation and Inflammation: A Vast Territory to Explore. *Front Endocrinol. (Lausanne)* **5**, 235 (2014).
 38. Ma, J. & Hart, G. W. Protein O-GlcNAcylation in diabetes and diabetic complications. *Expert Rev. Proteom.* **10**, 365–380 (2013).
 39. Louati, K., Vidal, C., Berenbaum, F. & Sellam, J. Association between diabetes mellitus and osteoarthritis: systematic literature review and meta-analysis. *RMD Open* **1**, e000077 (2015).
 40. Veronese, N. et al. Type 2 diabetes mellitus and osteoarthritis. *Semin Arthritis Rheum.* **49**, 9–19 (2019).
 41. Song, Z. Roles of the nucleotide sugar transporters (SLC35 family) in health and disease. *Mol. Asp. Med* **34**, 590–600 (2013).
 42. Hiraoka, S. et al. Nucleotide-sugar transporter SLC35D1 is critical to chondroitin sulfate synthesis in cartilage and skeletal development in mouse and human. *Nat. Med* **13**, 1363–1367 (2007).
 43. Kciuk, M. et al. Doxorubicin—An Agent with Multiple Mechanisms of Anticancer Activity. *Cells* **12**, <https://doi.org/10.3390/cells12040659> (2023).
 44. Allawzi, A., Elajaili, H., Redente, E. F. & Nozik-Grayck, E. Oxidative Toxicology of Bleomycin: Role of the Extracellular Redox Environment. *Curr. Opin. Toxicol.* **13**, 68–73 (2019).
 45. Tardio, L. et al. O-linked N-acetylglucosamine (O-GlcNAc) protein modification is increased in the cartilage of patients with knee osteoarthritis. *Osteoarthr. Cartil.* **22**, 259–263 (2014).
 46. Andres-Bergos, J. et al. The increase in O-linked N-acetylglucosamine protein modification stimulates chondrogenic differentiation both in vitro and in vivo. *J. Biol. Chem.* **287**, 33615–33628 (2012).
 47. Dreier, R. Hypertrophic differentiation of chondrocytes in osteoarthritis: the developmental aspect of degenerative joint disorders. *Arthritis Res Ther.* **12**, 216 (2010).
 48. Herrero-Beaumont, G. & Largo, R. Glucosamine and O-GlcNAcylation: a novel immunometabolic therapeutic target for OA and chronic, low-grade systemic inflammation? *Ann. Rheum. Dis.* **79**, 1261–1263 (2020).
 49. Kim, E. J. Advances in Strategies and Tools Available for Interrogation of Protein O-GlcNAcylation. *ChemBiochem* **22**, 3010–3026 (2021).
 50. Ma, H. L. et al. Osteoarthritis severity is sex dependent in a surgical mouse model. *Osteoarthr. Cartil.* **15**, 695–700 (2007).
 51. Roman-Blas, J. A., Castaneda, S., Largo, R. & Herrero-Beaumont, G. Osteoarthritis associated with estrogen deficiency. *Arthritis Res Ther.* **11**, 241 (2009).
 52. Martin-Millan, M. & Castaneda, S. Estrogens, osteoarthritis and inflammation. *Jt. Bone Spine* **80**, 368–373 (2013).
 53. Srikanth, V. K. et al. A meta-analysis of sex differences prevalence, incidence and severity of osteoarthritis. *Osteoarthr. Cartil.* **13**, 769–781 (2005).
 54. Nair, A. B. & Jacob, S. A simple practice guide for dose conversion between animals and human. *J. Basic Clin. Pharm.* **7**, 27–31, (2016).
 55. Altman, R. D. Glucosamine therapy for knee osteoarthritis: pharmacokinetic considerations. *Expert Rev. Clin. Pharm.* **2**, 359–371 (2009).
 56. McCarty, M. F., O’Keefe, J. H. & DiNicolantonio, J. J. Glucosamine for the Treatment of Osteoarthritis: The Time Has Come for Higher-Dose Trials. *J. Diet. Suppl.* **16**, 179–192 (2019).
 57. Weimer, S. et al. D-Glucosamine supplementation extends life span of nematodes and of ageing mice. *Nat. Commun.* **5**, 3563 (2014).
 58. Riegger, J., Baumert, J., Zaucke, F. & Brenner, R. E. The Hexosamine Biosynthetic Pathway as a Therapeutic Target after Cartilage Trauma: Modification of Chondrocyte Survival and Metabolism by Glucosamine Derivatives and PUGNAc in an Ex Vivo Model. *Int. J. Mol. Sci.* **22**, <https://doi.org/10.3390/ijms22147247> (2021).
 59. Varghese, S. et al. Glucosamine modulates chondrocyte proliferation, matrix synthesis, and gene expression. *Osteoarthr. Cartil.* **15**, 59–68 (2007).
 60. Clegg, D. O. et al. Glucosamine, chondroitin sulfate, and the two in combination for painful knee osteoarthritis. *N. Engl. J. Med* **354**, 795–808 (2006).
 61. Herrero-Beaumont, G. et al. Glucosamine sulfate in the treatment of knee osteoarthritis symptoms: a randomized, double-blind, placebo-controlled study using acetaminophen as a side comparator. *Arthritis Rheum.* **56**, 555–567 (2007).
 62. Pritzker, K. P. et al. Osteoarthritis cartilage histopathology: grading and staging. *Osteoarthr. Cartil.* **14**, 13–29 (2006).

63. Glasson, S. S., Blanchet, T. J. & Morris, E. A. The surgical destabilization of the medial meniscus (DMM) model of osteoarthritis in the 129/SvEv mouse. *Osteoarthr. Cartil.* **15**, 1061–1069 (2007).
64. Glasson, S. S., Chambers, M. G., Van Den Berg, W. B. & Little, C. B. The OARSI histopathology initiative - recommendations for histological assessments of osteoarthritis in the mouse. *Osteoarthr. Cartil.* **18**, S17–S23 (2010).
65. Little, C. B. et al. Matrix metalloproteinase 13-deficient mice are resistant to osteoarthritic cartilage erosion but not chondrocyte hypertrophy or osteophyte development. *Arthritis Rheum.* **60**, 3723–3733 (2009).
66. Armstrong, A. R., Carlson, C. S., Rendahl, A. K. & Loeser, R. F. Optimization of histologic grading schemes in spontaneous and surgically-induced murine models of osteoarthritis. *Osteoarthr. Cartil.* **29**, 536–546 (2021).
67. Hayer, S. et al. SMASH' recommendations for standardised microscopic arthritis scoring of histological sections from inflammatory arthritis animal models. *Ann. Rheum. Dis.* **80**, 714–726 (2021).
68. Goldring, M. B. Human chondrocyte cultures as models of cartilage-specific gene regulation. *Methods Mol. Med.* **107**, 69–95 (2005).
69. Gosset, M., Berenbaum, F., Thirion, S. & Jacques, C. Primary culture and phenotyping of murine chondrocytes. *Nat. Protoc.* **3**, 1253–1260 (2008).
70. Chen, Q., Fischer, A., Reagan, J. D., Yan, L. J. & Ames, B. N. Oxidative DNA damage and senescence of human diploid fibroblast cells. *Proc. Natl Acad. Sci. USA* **92**, 4337–4341 (1995).
71. Busutil, R. A., Rubio, M., Dolle, M. E., Campisi, J. & Vijg, J. Oxygen accelerates the accumulation of mutations during the senescence and immortalization of murine cells in culture. *Aging Cell* **2**, 287–294 (2003).
72. Parrinello, S. et al. Oxygen sensitivity severely limits the replicative lifespan of murine fibroblasts. *Nat. Cell Biol.* **5**, 741–747 (2003).
73. Finger, F. et al. Molecular phenotyping of human chondrocyte cell lines T/C-28a2, T/C-28a4, and C-28/I2. *Arthritis Rheum.* **48**, 3395–3403 (2003).
74. Barthel, S. R. et al. Peracetylated 4-fluoro-glucosamine reduces the content and repertoire of N- and O-glycans without direct incorporation. *J. Biol. Chem.* **286**, 21717–21731 (2011).
75. Shevchenko, A., Tomas, H., Havlis, J., Olsen, J. V. & Mann, M. In-gel digestion for mass spectrometric characterization of proteins and proteomes. *Nat. Protoc.* **1**, 2856–2860 (2006).
76. Debaq-Chainiaux, F., Erusalimsky, J. D., Campisi, J. & Toussaint, O. Protocols to detect senescence-associated beta-galactosidase (SA- β gal) activity, a biomarker of senescent cells in culture and in vivo. *Nat. Protoc.* **4**, 1798–1806 (2009).
77. Dobin, A. et al. STAR: ultrafast universal RNA-seq aligner. *Bioinformatics* **29**, 15–21 (2013).
78. Perteira, M. et al. StringTie enables improved reconstruction of a transcriptome from RNA-seq reads. *Nat. Biotechnol.* **33**, 290–295 (2015).
79. Love, M. I., Huber, W. & Anders, S. Moderated estimation of fold change and dispersion for RNA-seq data with DESeq2. *Genome Biol.* **15**, 550 (2014).
80. Subramanian, A. et al. Gene set enrichment analysis: a knowledge-based approach for interpreting genome-wide expression profiles. *Proc. Natl Acad. Sci. USA* **102**, 15545–15550 (2005).
81. Dunn, S. L. et al. Gene expression changes in damaged osteoarthritic cartilage identify a signature of non-chondrogenic and mechanical responses. *Osteoarthr. Cartil.* **24**, 1431–1440 (2016).
82. Kramer, A., Green, J., Pollard, J. Jr. & Tugendreich, S. Causal analysis approaches in Ingenuity Pathway Analysis. *Bioinformatics* **30**, 523–530 (2014).
83. Cornelis, F. M. F. et al. ANP32A regulates ATM expression and prevents oxidative stress in cartilage, brain, and bone. *Sci. Transl. Med.* **10**, <https://doi.org/10.1126/scitranslmed.aar8426> (2018).
84. Choi, W. S. et al. The CH25H-CYP7B1-ROR α axis of cholesterol metabolism regulates osteoarthritis. *Nature* **566**, 254 (2019).
85. Deng, Y. et al. Reciprocal inhibition of YAP/TAZ and NF- κ B regulates osteoarthritic cartilage degradation. *Nat. Commun.* **9**, 4564 (2018).
86. Kim, J. H. et al. Regulation of the catabolic cascade in osteoarthritis by the zinc-ZIP8-MTF1 axis. *Cell* **156**, 730–743 (2014).
87. Kang, D. et al. Selenophosphate synthetase 1 deficiency exacerbates osteoarthritis by dysregulating redox homeostasis. *Nat. Commun.* **13**, 779 (2022).

Acknowledgements

This work was supported by grants from the National Research Foundation (NRF) of Korea (RS-2024-00345291 to D.K., NRF-2022R1A6A3A13071341 to J.L., RS-2023-NR077245, and NRF-2016R1A5A1010764 to J.-H.K.), Korea Drug Development Fund funded by Ministry of Science and ICT (MSIT), Ministry of Trade, Industry, and Energy, and Ministry of Health and Welfare (RS-2023-00217266 to J.-H.K.), Bio&Medical Technology Development Program of the NRF funded by the Korean government (MSIT) (RS-2024-00440273 to J.-H.K.), the Institute for Basic Science from the Ministry of Science, ICT and Future Planning of Korea (IBS-R008-D1 to J.-H.K.), and Suh Kyungbae foundation (to J.-H.K.).

Author contributions

D.K., J.L., and J.-H.K. designed the study. D.K. and J.L. performed most in vitro experiments and animal experiments. D.K. and G.Y. performed bioinformatic analysis of RNA sequencing data. S.J. and J.S. performed several repeat experiments. H.J., J.A., and E.C.Y. performed MS experiments and analysis. T.W.K., M.J.C., C.B.C., and S.-B.K. collected and inspected human patient samples. M.-S.K., Y.-J.K., W.H.Y., Y.-h.L., J.W.C., and C.K. contributed materials/analytical tools and provided intellectual input to project design and data interpretation. D.K., J.L., E.C.Y., C.K., and J.-H.K. analyzed the data. D.K., J.L., and J.-H.K. wrote the original draft of the manuscript. All authors read and edited the manuscript. J.-H.K. supervised the study.

Competing interests

The authors declare the following competing interests: Y.-J.K. and J.-H.K. are co-founders of Liflex Science. D.K., J.L., C.K., and J.-H.K. are the inventors of a patent application based on this study (South Korea patent pending, No. 10-2024-0155038). The other authors declare no competing interests.

Additional information

Supplementary information The online version contains supplementary material available at <https://doi.org/10.1038/s41467-024-55085-1>.

Correspondence and requests for materials should be addressed to Jin-Hong Kim.

Peer review information *Nature Communications* thanks Gabriel Herrero-Beaumont, Richard Loeser and the other, anonymous, reviewer(s) for their contribution to the peer review of this work. A peer review file is available.

Reprints and permissions information is available at <http://www.nature.com/reprints>

Publisher's note Springer Nature remains neutral with regard to jurisdictional claims in published maps and institutional affiliations.

Open Access This article is licensed under a Creative Commons Attribution-NonCommercial-NoDerivatives 4.0 International License, which permits any non-commercial use, sharing, distribution and reproduction in any medium or format, as long as you give appropriate credit to the original author(s) and the source, provide a link to the Creative Commons licence, and indicate if you modified the licensed material. You do not have permission under this licence to share adapted material derived from this article or parts of it. The images or other third party material in this article are included in the article's Creative Commons licence, unless indicated otherwise in a credit line to the material. If material is not included in the article's Creative Commons licence and your intended use is not permitted by statutory regulation or exceeds the permitted use, you will need to obtain permission directly from the copyright holder. To view a copy of this licence, visit <http://creativecommons.org/licenses/by-nc-nd/4.0/>.

© The Author(s) 2025

¹Department of Biological Sciences, College of Natural Sciences, Seoul National University, Seoul 08826, South Korea. ²Center for RNA Research, Institute for Basic Science, Seoul 08826, South Korea. ³Department of Environmental Medicine, College of Medicine, Ewha Womans University, Seoul 07985, South Korea. ⁴Department of Molecular Medicine and Biopharmaceutical Sciences, School of Convergence Science and Technology, College of Medicine, Seoul National University, Seoul 03080, South Korea. ⁵Department of Orthopaedic Surgery, Seoul National University Boramae Hospital, Seoul 07061, South Korea. ⁶Department of Orthopaedic Surgery, Seoul National University Bundang Hospital, Seongnam 13620, South Korea. ⁷Department of Systems Biology, College of Life Science and Biotechnology, Yonsei University, Seoul 03722, South Korea. ⁸Glycosylation Network Research Center, Yonsei University, Seoul 03722, South Korea. ⁹Department of Internal Medicine, Yonsei University College of Medicine, Seoul 03722, South Korea. ¹⁰Institute of Green-Bio Science and Technology, Seoul National University, Pyeongchang 25354, South Korea. ¹¹Interdisciplinary Program in Bioinformatics, Seoul National University, Seoul 08826, South Korea. ¹²These authors contributed equally: Donghyun Kang, Jeeyeon Lee. ✉ e-mail: jinhkim@snu.ac.kr